SAR COMPLIANCE TESTING OF D-LINK CORPORATION AIRPRO DUAL-BAND
WIRELESS CARDBUS ADAPTER MODEL DWL-AG650 INSERTED INTO
AN IBM LAPTOP COMPUTER

FCC ID: KA2DWL-AG650A1

HOST COMPUTER: IBM Model 2659

March 27, 2003

Prepared for: D-Link Corporation
                     No. 8, Li-Hsin VII Road
                     Science-Based Industrial Park
                     Hsin-Chu, Taiwan, R.O.C.

Prepared by: Om P. Gandhi
                     Professor of Electrical and Computer Engineering
                     University of Utah
                     50 S Central Campus Dr., Rm. 3280
                     Salt Lake City, UT 84112-9206

TABLE OF CONTENTS

SAR COMPLIANCE TESTING OF D-LINK CORPORATION AIRPRO DUAL-BAND
WIRELESS CARDBUS ADAPTER MODEL DWL-AG650 INSERTED INTO
AN IBM LAPTOP COMPUTER

FCC ID: KA2DWL-AG650A1
HOST COMPUTER: IBM Model 2659

I. Introduction

The U.S. Federal Communications Commission (FCC) has adopted limits of human exposure to RF emissions from mobile and portable devices that are regulated by the FCC [1]. The FCC has also issued Supplement C (Edition 97-01) to OET Bulletin 65 [2] and a more recent version of the same [3] defining both the measurement and the computational procedures that should be followed for evaluating compliance of mobile and portable devices with FCC limits for human exposure to radiofrequency emissions.

We have used the measurement procedure for SAR compliance testing of the D-Link Corporation AirPro Dual-Band Wireless Cardbus Adapter Model DWL-AG650 inserted into an IBM Laptop Computer (FCC ID# KA2DWL-AG650A1).   Photographs of the unit with the Cardbus Card inserted into the laptop computer are given in Figs. 1a-c for top and bottom sides of the PC and for the side view, respectively.   A picture of the Cardbus Card placed on the laptop is given in Fig. 2. The D-Link Model DWL-AG650 Cardbus Adapter operates over the frequency band 5.18 to 5.805 GHz in normal mode with conducted powers given in Table 1.

For SAR measurements, two configurations of the wireless PC relative to the experimental phantom have been used. These are as follows:

a. **Configuration 1** is for the wireless PC placed on a user's lap. For this configuration, a planar phantom model with inside dimensions 12" × 16.5" (30.5 × 41.9 cm) and a base thickness of 2.0 ± 0.2 mm (recommended in [3]) was used for SAR measurements and the bottom side of the laptop computer shown in Fig. 1b was pressed against it (see Fig. 3). For this configuration, the distance from the base of the cardbus card to the base of the PC is approximately 1.14 cm.

b. **Configuration 2** -- Edge-on position. This configuration corresponds to a bystander close to the edge of the cardbus card at a distance of 0 cm. For this configuration, the PC base is placed at 90° with the card edge pressed against the bottom of the phantom (see Fig. 4) at a distance of 0 cm as shown.

II. The SAR Measurement System

The University of Utah SAR Measurement System has been described in peer-reviewed literature [Ref. 8 -- attached here as Appendix A]. A photograph of the SAR Measurement System is given in Fig. 5. This SAR Measurement System uses a computer-controlled 3-D stepper motor system (Arrick Robotics MD-2A). A triaxial Narda Model 8021 E-field probe is used to determine the internal electric fields. The positioning repeatability of the stepper motor system moving the E-field probe is within ±0.1 mm. Outputs from the three channels of the E-field probe are dc voltages, the sum of which is proportional to the square of the internal electric fields $\left(|E_i|^2\right)$ from which the SAR can be obtained from the equation SAR = $\sigma\left(|E_i|^2\right)\big/\rho$, where σ and ρ are the conductivity and mass density of the tissue-simulant materials, respectively [5]. The dc voltages for the three channels of the E-field probe are read by three HP 34401A multimeters and sent to the computer via an HPIB interface. The setup is carefully grounded and shielded to reduce the noise due to the electromagnetic interference (EMI). A cutout in a wooden table of dimensions 38.1 × 21.6 cm allows placement of a plastic holder (shown in Fig. 6) on which the laptop computer with the Cardbus Adapter (see Fig. 1) is supported. A plastic holder (see Fig. 6) can be moved up or down so that the base of the PC (for Configuration 1) is pressed against the base of the flat phantom for determination of SAR for Above-Lap position. Similarly, for "Edge-On" SAR determination, Configuration 2, the laptop computer is mounted sideways (at 90°) on the plastic holder and moved up so that the card edge was pressed against the bottom of the flat phantom with a spacing of 0 cm (see Fig. 4).

The Flat Phantom

As recommended in Supplement C Edition 01-01 to OET Bulletin 65 [3], a planar phantom model with inside dimensions 12" × 16.5" (30.5 × 41.9 cm) and base thickness 2.0 ± 0.2 mm was used for SAR measurements (see Figs. 3, 4).

III. Calibration of the E-Field Probe

The IEEE Draft Standard P1528 [4] suggests a recommended procedure for probe calibration (see Section 4.4.1 of [4]) for frequencies above 800 MHz where waveguide size is manageable. Calibration using a rectangular waveguide is recommended. As in some previously reported SAR measurements at 6 GHz [5], we have calibrated the Narda Model 8021 Miniature Broadband Electric Field Probe of tip diameter 4 mm (internal dipole dimensions on the order of 2.5 mm) using a rectangular waveguide WR 159 (of internal dimensions 1.59 x 0.795 inches) that was filled with the tissue-simulant fluid of composition given in Section V (see Figs. 7a, b). The triaxial (3 dipole) E-field probe shown in Fig. 8 was originally developed by Howard Bassen and colleagues of FDA and has been manufactured under license by Narda Microwave Corporation, Hauppage, New York. The probe is described in detail in references 6 and 7. It uses three orthogonal pick up dipoles each of length about 2.5 mm offset from the tip by 3 mm, each with its own leadless zero voltage Schottky barrier diode operating in the square law region. The sum of the three diode outputs read by three microvoltmeters [8] gives an output proportional to E^2. By rotating the probe around its axis, the isotropy of the probe was measured to be less than ± 0.23 dB and the deviation of the probe from the square law behavior was less than ± 3%.

As suggested in the Draft Standard P1528, the waveguide (WR 159) filled with the tissue-simulant fluid was maintained vertically. From microwave field theory [see e.g. ref. 9], the transverse field distribution in the liquid corresponds to the fundamental mode (TE_{10}) with an exponential decay in the vertical direction (z-axis). The liquid level was 15 cm deep which is deep enough to guarantee that reflections from the top liquid surface do not affect the calibration.

By comparing the square of the decaying electric fields expected in the tissue from the analytical expressions for the TE_{10} mode of the rectangular waveguide, we obtained a calibration factor of 2.98 (mW/kg)/μV with a variability of less than ±2% for measurement frequencies of 5.25 and 5.8 GHz, respectively. This is no doubt due to a fairly limited frequency band of only 0.55 GHz out of a recommended bandwidth of 2.2 GHz for the TE_{10} mode for the WR159 waveguide (recommended band of 4.9-7.1 GHz -- see e.g. ref. 9) and the fact that the bandwidth of 550 MHz for the entire set of measurements is on the order of ± 5% of the midband frequencies..

The date for the calibration of the E-field probe closest to the SAR tests given here was March 24, 2003.

IV. SAR System Verification

Since we do not have a dipole for the 5 GHz band, a half wave dipole at 1900 MHz was used instead for SAR system verification.[1] This dipole of length 76.0 mm and diameter 1.5 mm and h = 39.5 mm is shown in Fig. 9. As recommended in OET65 Supplement C [3], we used a spacing of 10 mm from the dipole to the tissue-simulant fluid composed of 40.4% water, 58.0% sugar, 0.5% salt (NaCl), 1% HEC, and 0.1% bactericide. The microwave circuit arrangement used for system verification is sketched in Fig. 10. The dielectric properties for this body-simulant fluid were measured using the Hewlett Packard (HP) Model 85070 B Dielectric Probe (rated frequency band 200 MHz to 20 GHz in conjunction with HP Model 8720C Network Analyzer (50 MHz-20 GHz) using a procedure detailed in Section V. The measured dielectric parameters of the body-simulant fluid at 1900 MHz are ε_r = 53.1 ± 1.3 and σ = 1.44 ± 0.09 S/m. The measured properties are close to the values of ε_r = 54.0 and σ = 1.45 S/m given in OET Supplement C [3].

The measured SAR distribution for the peak 1-g SAR region using this system verification dipole for the day of SAR measurements, March 24, 2003, is given in Appendix B.

---

[1] Use of an open-ended, air-filled waveguide is an appropriate substitute for a hard-to-fabricate dipole in the 5-5.8 GHz band. We are presently developing this system for SAR system verification at 5.25 and 5.8 GHz. This development will be completed by the first week of April 2003.

Also given in Appendix B is the dipole SAR plot for this date of device testing. The peak 1-g SAR is 35.459 W/kg. The measured 1-g SAR is in excellent agreement with the FDTD-calculated 1-g SAR of 35.8 W/kg for this dipole. Also as expected, the measured SAR plot is quite symmetric.

V. Tissue Simulant Fluid for the Frequency Band 5.2 to 5.8 GHz

In OET 65 Supplement C [3], the dielectric parameters suggested for body phantom are given only for 3000 and 5800 MHz. These are listed in Table 2 here. Using linear interpolation, we can obtain the dielectric parameters to use for the frequency band between 5.2 to 5.8 GHz. The desired dielectric properties thus obtained are also given in Table 2. From Table 2, it can be noticed that the desired dielectric constant ε_r varies from 48.2 to 49.0 which is a variation of less than $\pm 1\%$ from the average value of 48.6 for this band. Also the conductivity σ varies linearly with frequency from 5.3 to 6.00 S/m. For the SAR measurements given in this report, we have used a tissue-simulant fluid developed at the University of Utah which consists of 68.0% water, 31.0% sugar and 1% HEC. For this composition, we have measured the dielectric properties using a Hewlett Packard (HP) Model 85070B Dielectric Probe in conjunction with HP Model 8720C Network Analyzer (50 MHz-20 GHz). The measured dielectric properties at a mid band frequency of 5.30 GHz are as follows: $\varepsilon_r = 48.5 \pm 1.7$ and $\sigma = 5.40 \pm 0.08$ S/m. From Table 2, we obtain the desired dielectric properties to simulate the body tissue at the midband frequency of 5.30 GHz to be $\varepsilon_r = 48.9$ and $\sigma = 5.42$ S/m. Thus, the measured properties for the body-simulant fluid are close to the desired values. Also as expected, the conductivity of this fluid varies linearly with frequency rising to 6.03 ± 0.09 S/m at 5.8 GHz, while the dielectric constant ε_r is nearly the same as the measured value at 5.3 GHz.

The procedure is as follows: The HP Model 95070B Dielectric Probe (see Fig. 11) is an open-circuited transmission-line (coaxial line) probe similar to that described in Section B.1.2 of the Draft IEEE Standard 1528 [4]. The theory of the open-circuited coaxial line method has been described in scientific literature [10-12]. We have previously used this method in

determining the dielectric properties of tissue-simulant materials at 6 GHz [5]. In this method, the complex reflection coefficient Γ^* measured for the open end of the coaxial line can be used to calculate the complex permittivity ε^* from the following equation [5]

$$\varepsilon^* = \frac{1-\Gamma^*}{j\omega Z_o C_o \left(1+\Gamma^*\right)} - \frac{C_f}{C_o} \tag{1}$$

where Z_o is the characteristic impedance (50 Ω) for the coaxial line, C_o is the capacitance when the line is in air and C_f is the capacitance that accounts for the fringing fields in the dielectric of the coaxial line.

For the HP85070B Dielectric Probe with diameters of the outer and inner conductors $2b = 3.00$ mm and $2a = 0.912$ mm, respectively, the following capacitances were obtained using deionized water and methanol as the calibration fluids. The following capacitances were obtained:

$$C_o = 0.022 \text{ pF}$$

$$C_f = 0.005 \text{ pF}$$

Using the network analyzer HP8720C, we measured the reflection coefficient Γ^* for the open end of the coaxial line that was submerged in the tissue-simulant fluid. Using Eq. 1, the complex permittivity of the fluid was measured at various frequencies 5.2-5.4 GHz. From the imaginary part of the complex permittivity $\text{Im}(\varepsilon^*)$, we can obtain the conductivity σ from the relationship

$$\sigma = \frac{\text{Im}(\varepsilon^*)}{\omega \varepsilon_o} \tag{2}$$

VI. The Measured SAR Distributions

The RF power output measured for the D-Link Model DWL-AG650 802.11a wireless antenna is given in Table 1. For SAR measurements, we selected frequencies of 5.26 and 5.805

6

GHz. These frequencies were selected both for their highest power outputs as well as to cover the different frequency modes planned for this wireless device. As recommended in Supplement C, Edition 01-01 [3], the stability of the conducted power was determined by repeated SAR measurements at the same location for each of the selected channels. The variability of the SAR thus determined for three repeated measurements over a 60-minute time period was within ± 0.1 dB (± 2.5%).

The highest SAR region for each of the measurement frequencies was identified in the first instance by using a coarser sampling with a step size of 8.0 mm over three overlapping areas for a total scan area of 8.0 × 9.6 cm. The data thus obtained is resolved into a 4 × 4 times larger grid i.e. a grid involving 40 × 28 points by linear interpolation using a 2 mm step size. After thus identifying the region of the highest SAR, the SAR distribution was then measured with a resolution of 2 mm in order to obtain the peak 1 cm^3 or 1-g SAR. The SAR measurements are performed at 4, 6, 8, 10, 12 mm height from the bottom surface of the body-simulant fluid. The SARs thus measured were extrapolated using a second-order least-square fit to the measured data to obtain values at 1, 3, 5, 7, and 9 mm height and used to obtain 1-g SARs. The uncertainty analysis of the University of Utah SAR measurement system is given in Appendix C. The combined standard uncertainty is ± 8.3%.

The coarse scans for the selected frequencies for configurations 1 and 2 are given in Figs. 12a, b and 13a, b, respectively. In these figures, the two axes are marked in units of the step size of 8 mm. The highest SAR region shown in maroon color is immediately above the region of the radiating antenna. Given in Tables 3-6 are the SAR distributions for the peak SAR region of volume 10 ×10 × 10 mm for which the coarse scans are given in Figs. 12a,b and 13a,b, respectively. The SARs are given for xy planes at heights z of 1, 3, 5, 7, and 9 mm from the bottom of the flat phantom. The individual SAR values for this grid of 5 × 5 × 5 or 125 points are averaged to obtain peak 1-g SAR values (for a volume of 1 cm^3). The temperature variation of the tissue-simulant fluid measured with a Bailey Instruments Model BAT 8 Temperature Probe over the 80-minute period needed for measurements at the four frequencies was 23.2 ±

$0.2^{\circ}C$. The z-axis scan plots taken at the highest SAR locations for each set of tests are given in Fig. 14 and 15, respectively.

The peak 1-g SARs for the various configurations of the D-Link Corporation AirPro Dual-Band Wireless Cardbus Adapter Model DWL-AG650 inserted into an IBM Model 2659 Laptop Computer (FCC ID# KA2DWL-AG650A1) are summarized in Table 7. All of the measured 1-g SARs are less than the FCC 96-326 guideline of 1.6 W/kg.

VII. Comparison of the Data with FCC 96-326 Guidelines

According to the FCC 96-326 Guideline [1], the peak SAR for any 1-g of tissue should not exceed 1.6 W/kg. For the D-Link Model DWL-AG650 Wireless Cardbus Adapter (FCC ID# KA2DWL-AG650A1), the measured peak 1-g SARs vary from 0.172 to 0.196 W/kg which are smaller than 1.6 W/kg.

REFERENCES

1. Federal Communications Commission, "Guidelines for Evaluating the Environmental Effects of Radiofrequency Radiation," FCC 96-326, August 1, 1996.

2. K. Chan, R. F. Cleveland, Jr., and D. L. Means, "Evaluating Compliance With FCC Guidelines for Human Exposure to Radiofrequency Electromagnetic Fields," Supplement C (Edition 97-01) to OET Bulletin 65, December, 1997. Available from Office of Engineering and Technology, Federal Communications Commission, Washington D.C., 20554.

3. Federal Communications Commission "Supplement C Edition 01-01 to OET Bulletin 65 Edition 97-01" June 2001.

4. IEEE Draft Standard P1528, "Recommended Practice for Determining the Peak Spatial-Average Specific Absorption Rate (SAR) in the Human Body Due to Wireless Communication Devices: Experimental Techniques," Draft CBD1.0, April 4, 2002 (IEEE Standards Coordinating Committee 34).

5. O. P. Gandhi and J-Y. Chen, "Electromagnetic Absorption in the Human Head from Experimental 6-GHz Handheld Transceivers," *IEEE Transactions on Electromagnetic Compatibility*, Vol. 39(4), pp. 547-558, 1995.

6. H. Bassen. M. Swicord, and J. Abita, "A Miniature Broadband Electric Field Probe," Ann. New York Academy of Sciences, Vol. 247, pp. 481-493, 1974.

7. H. Bassen and T. Babij, "Experimental Techniques and Instrumentation," Chapter 7 in *Biological Effects and Medical Applications of Electromagnetic Energy*, O. P. Gandhi, Editor, Prentice Hall Inc., Englewood Cliffs, NJ, 1990.

8. Q. Yu, O. P. Gandhi, M. Aronsson, and D. Wu, "An Automated SAR Measurement System for Compliance Testing of Personal Wireless Devices," *IEEE Transactions on Electromagnetic Compatibility,* Vol. 41(3), pp. 234-245, August 1999 (attached as Appendix A).

9. O. P. Gandhi, *Microwave Engineering and Applications,* Pergamon Press, New York, 1981.

10. T. W. Athey, M. A. Stuchly, and S. S. Stuchly, "Measurement of Radiofrequency Permittivity of Biological Tissues with an Open-Circuited Coaxial Line - Part I," *IEEE Transactions on Microwave Theory and Techniques*, Vol. MTT-30, pp. 82-86, 1982.

11. M. A. Stuchly, T. W. Athey, G. M. Samaras, and G. E. Taylor, "Measurement of Radiofrequency Permittivity of Biological Tissues with an Open-Circuited Coaxial Line - Part II - Experimental Results," *IEEE Transactions on Microwave Theory and Techniques*, Vol. MTT-30, pp. 87-92, 1982.

12. C. L. Pournaropoulos and D. K. Misra, "The Coaxial Aperture Electromagnetic Sensor and Its Application for Material Characterization," *Measurement Science and Technology*, Vol. 8, pp. 1191-1202, 1997.

Table 1.   Conducted RF power outputs measured at various frequencies for the D-Link
           Model DWL-AG650 Wireless Cardbus Adapter for the normal mode.

Normal Mode		
Channel	Frequency GHz	Conducted Output Power dBm
1	5.18	15.57
4	5.24	15.54
5	5.26	16.83
8	5.32	16.77
9	5.745	14.97
12	5.805	16.21

Table 2.   Dielectric parameters for body phantom for the frequency band 5.2 to 5.8 GHz [3].

Frequency GHz	ε_r	σ S/m	Reference
3.0	52.0	2.73	Ref. 3
5.8	48.2	6.00	Ref. 3
5.2	49.0	5.30	Interpolated
5.3	48.9	5.42	Interpolated
5.4	48.7	5.53	Interpolated
5.6	48.5	5.77	Interpolated
5.7	48.3	5.88	Interpolated

Table 3. **Above-lap position (Configuration 1).** The SARs measured for the D-Link Model DWL-AG650 Wireless Cardbus Adapter for the normal mode at 5.26 GHz.

1-g SAR = 0.196 W/kg

a. At depth of 1 mm

0.209	0.234	0.228	0.208	0.227
0.250	0.251	0.230	0.251	0.235
0.234	0.228	0.211	0.234	0.263
0.230	0.269	0.270	0.225	0.234
0.230	0.247	0.221	0.245	0.263

b. At depth of 3 mm

0.187	0.205	0.204	0.195	0.200
0.223	0.215	0.207	0.214	0.209
0.206	0.211	0.198	0.212	0.229
0.213	0.228	0.230	0.211	0.213
0.204	0.212	0.203	0.216	0.229

c. At depth of 5 mm

0.172	0.183	0.185	0.185	0.180
0.200	0.187	0.189	0.187	0.188
0.185	0.197	0.187	0.194	0.203
0.198	0.197	0.199	0.199	0.194
0.183	0.186	0.188	0.193	0.203

d. At depth of 7 mm

0.164	0.167	0.173	0.177	0.166
0.182	0.168	0.175	0.169	0.174
0.169	0.184	0.178	0.182	0.184
0.187	0.174	0.178	0.188	0.179
0.169	0.168	0.174	0.178	0.183

e. At depth of 9 mm

0.162	0.158	0.167	0.171	0.159
0.169	0.157	0.165	0.162	0.166
0.160	0.174	0.171	0.173	0.172
0.179	0.160	0.167	0.178	0.166
0.160	0.158	0.163	0.169	0.170

Table 4.　**Above-lap position (Configuration 1).** The SARs measured for the D-Link Model DWL-AG650 Wireless Cardbus Adapter for the normal mode at 5.805 GHz.

1-g SAR = 0.177 W/kg

a. At depth of 1 mm

0.194	0.161	0.211	0.215	0.220
0.205	0.211	0.215	0.240	0.233
0.222	0.224	0.217	0.203	0.259
0.205	0.136	0.196	0.218	0.215
0.167	0.145	0.226	0.163	0.081

b. At depth of 3 mm

0.186	0.171	0.191	0.193	0.199
0.190	0.191	0.197	0.205	0.211
0.194	0.195	0.197	0.190	0.223
0.188	0.152	0.177	0.196	0.191
0.165	0.154	0.187	0.164	0.115

c. At depth of 5 mm

0.179	0.176	0.175	0.175	0.182
0.178	0.176	0.183	0.181	0.192
0.173	0.174	0.182	0.180	0.196
0.176	0.163	0.164	0.179	0.173
0.162	0.160	0.160	0.162	0.138

d. At depth of 7 mm

0.172	0.176	0.166	0.163	0.171
0.168	0.165	0.172	0.167	0.177
0.158	0.161	0.171	0.172	0.177
0.169	0.170	0.157	0.166	0.160
0.160	0.162	0.145	0.160	0.150

e. At depth of 9 mm

0.166	0.172	0.161	0.157	0.163
0.162	0.159	0.165	0.164	0.166
0.151	0.156	0.165	0.168	0.166
0.165	0.172	0.158	0.158	0.152
0.158	0.161	0.142	0.155	0.151

Table 5.   **Edge-on position (Configuration 2).**   The SARs measured for the D-Link Model DWL-AG650 Wireless Cardbus Adapter for the normal mode at 5.26 GHz.

1-g SAR = 0.172 W/kg

a. At depth of 1 mm

0.182	0.193	0.195	0.202	0.165
0.201	0.211	0.198	0.185	0.210
0.197	0.192	0.205	0.190	0.175
0.187	0.196	0.199	0.199	0.181
0.211	0.193	0.180	0.186	0.193

b. At depth of 3 mm

0.178	0.182	0.179	0.177	0.156
0.180	0.188	0.184	0.178	0.188
0.185	0.183	0.190	0.175	0.167
0.178	0.184	0.187	0.187	0.172
0.191	0.179	0.171	0.177	0.179

c. At depth of 5 mm

0.174	0.172	0.167	0.157	0.149
0.165	0.170	0.173	0.172	0.172
0.175	0.175	0.178	0.164	0.160
0.171	0.174	0.178	0.177	0.165
0.175	0.167	0.165	0.170	0.168

d. At depth of 7 mm

0.170	0.162	0.158	0.144	0.144
0.155	0.156	0.165	0.167	0.161
0.167	0.167	0.168	0.157	0.154
0.165	0.166	0.171	0.168	0.159
0.166	0.160	0.162	0.164	0.159

e. At depth of 9 mm

0.166	0.153	0.151	0.137	0.141
0.150	0.147	0.159	0.164	0.155
0.161	0.161	0.162	0.153	0.150
0.161	0.160	0.167	0.161	0.155
0.161	0.156	0.162	0.160	0.154

Table 6.   **Edge-on position (Configuration 2).** The SARs measured for the D-Link Model DWL-AG650 Wireless Cardbus Adapter for the normal mode at 5.805 GHz.

1-g SAR = 0.175 W/kg

a. At depth of 1 mm

0.188	0.191	0.204	0.194	0.179
0.223	0.206	0.206	0.195	0.187
0.206	0.195	0.172	0.171	0.186
0.179	0.183	0.172	0.194	0.215
0.209	0.187	0.202	0.180	0.187

b. At depth of 3 mm

0.179	0.182	0.189	0.182	0.176
0.198	0.189	0.189	0.175	0.180
0.185	0.179	0.168	0.174	0.177
0.175	0.172	0.170	0.182	0.191
0.191	0.181	0.186	0.178	0.181

c. At depth of 5 mm

0.172	0.175	0.178	0.173	0.172
0.178	0.176	0.176	0.161	0.174
0.169	0.167	0.164	0.175	0.170
0.171	0.163	0.168	0.173	0.173
0.178	0.175	0.174	0.176	0.175

d. At depth of 7 mm

0.166	0.170	0.170	0.167	0.169
0.166	0.166	0.166	0.152	0.168
0.158	0.158	0.159	0.174	0.165
0.167	0.156	0.166	0.166	0.160
0.169	0.171	0.166	0.174	0.171

e. At depth of 9 mm

0.162	0.165	0.167	0.164	0.166
0.160	0.158	0.158	0.149	0.164
0.152	0.151	0.155	0.170	0.162
0.162	0.151	0.164	0.161	0.154
0.165	0.167	0.161	0.172	0.167

Table 7.   The peak 1-g SARs measured for the D-Link Model DWL-AG650 Wireless Cardbus Adapter inserted into an IBM Model 2659 Notebook Computer (FCC ID# KA2DWL-AG650A1).

1-g SAR in W/kg

PC position relative to the flat phantom	Spacing to the bottom of the phantom	5.26 GHz Normal Mode	5.805 GHz Normal Mode
Configuration 1 – "Above-lap" position; bottom of PC pressed against bottom of the flat phantom (see Fig. 3)	0 cm	0.196	0.177
Configuration 2 – "Edge-on" placement; PC at 90° with the card edge at a distance of 0 cm from the base of the phantom (see Fig. 4)	0 cm	0.172	0.175

a. Top side of the laptop computer.

Fig. 1. Photograph of the D-Link Model DWL-AG650 Cardbus Adapter inserted into an IBM Model 2659 laptop computer.

b. Bottom side of the laptop computer.

Fig. 1. Photograph of the D-Link Model DWL-AG650 Cardbus Adapter inserted into an IBM Model 2659 laptop computer.

c. Side view – Cardbus Adapter inserted into the PC.

Fig. 1.   Photograph of the D-Link Model DWL-AG650 Cardbus Adapter inserted
            into an IBM Model 2659 laptop computer.

Fig. 2.   A picture of the D-Link Model DWL-AG650 Cardbus Adapter placed on
the IBM laptop computer.
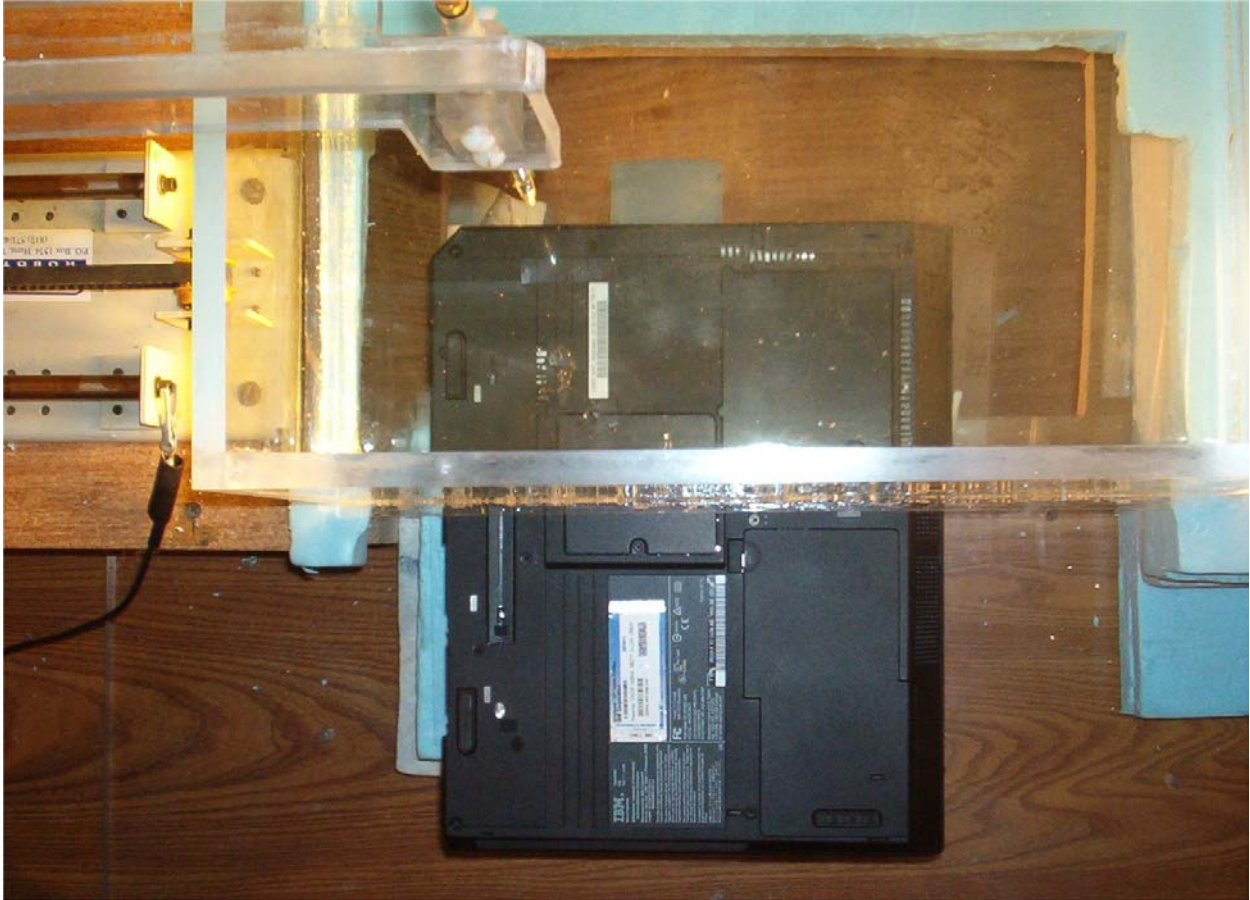
Fig. 3.   Photograph of the D-Link Model DWL-AG650 Cardbus Adapter inserted into an IBM Laptop Computer with its bottom pressed against the bottom of the planar phantom. This is **Configuration 1** – Laptop position for SAR testing.

Fig. 4. Photograph of the D-Link Model DWL-AG650 Cardbus Adapter inserted into an IBM Laptop Computer placed with the card edge at 90° pressed against the base of the planar phantom. This is **Configuration 2** for SAR testing and represents the case of a bystander in contact (at a spacing of 0 cm) from the card edge.
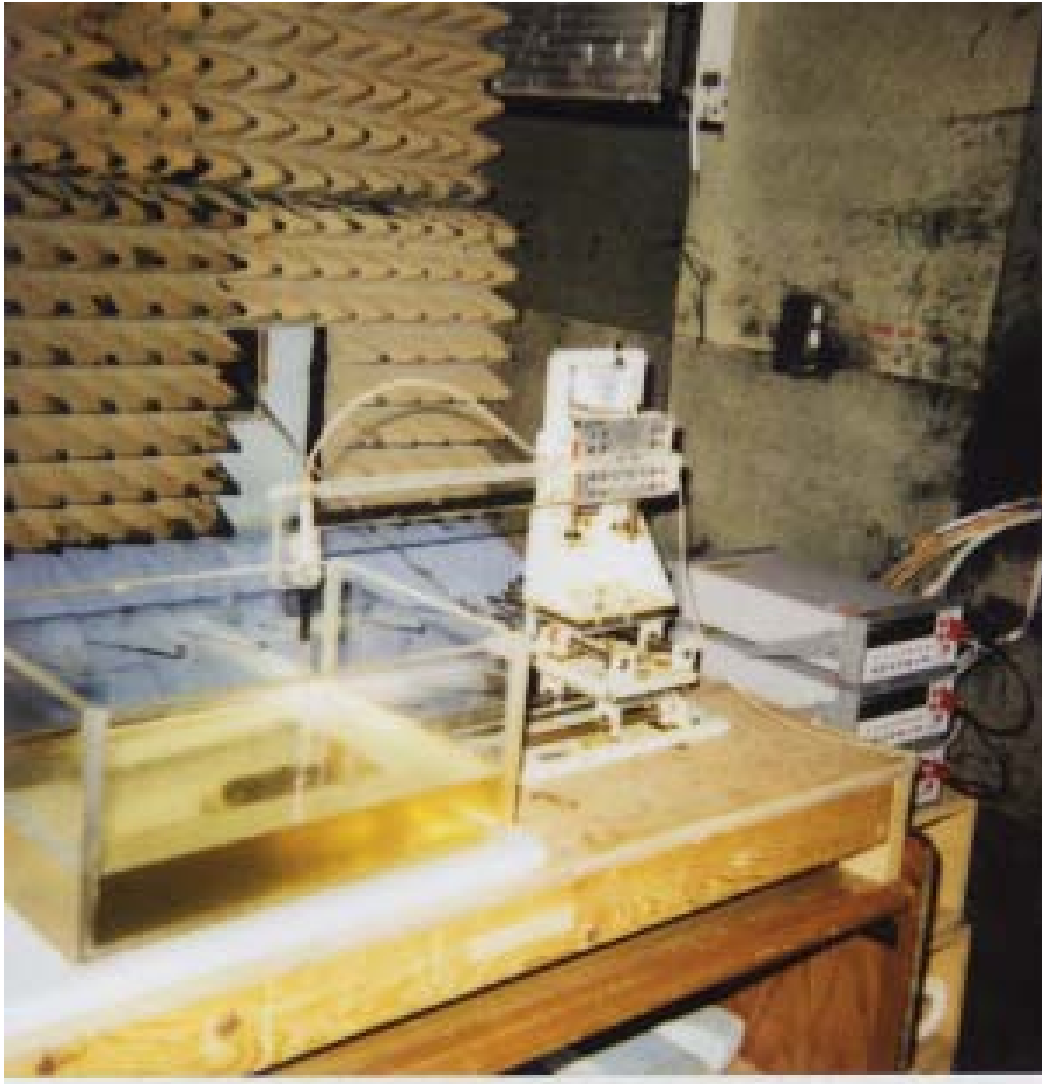
Fig. 5. Photograph of the three-dimensional stepper-motor-controlled SAR measurement system using a planar phantom.
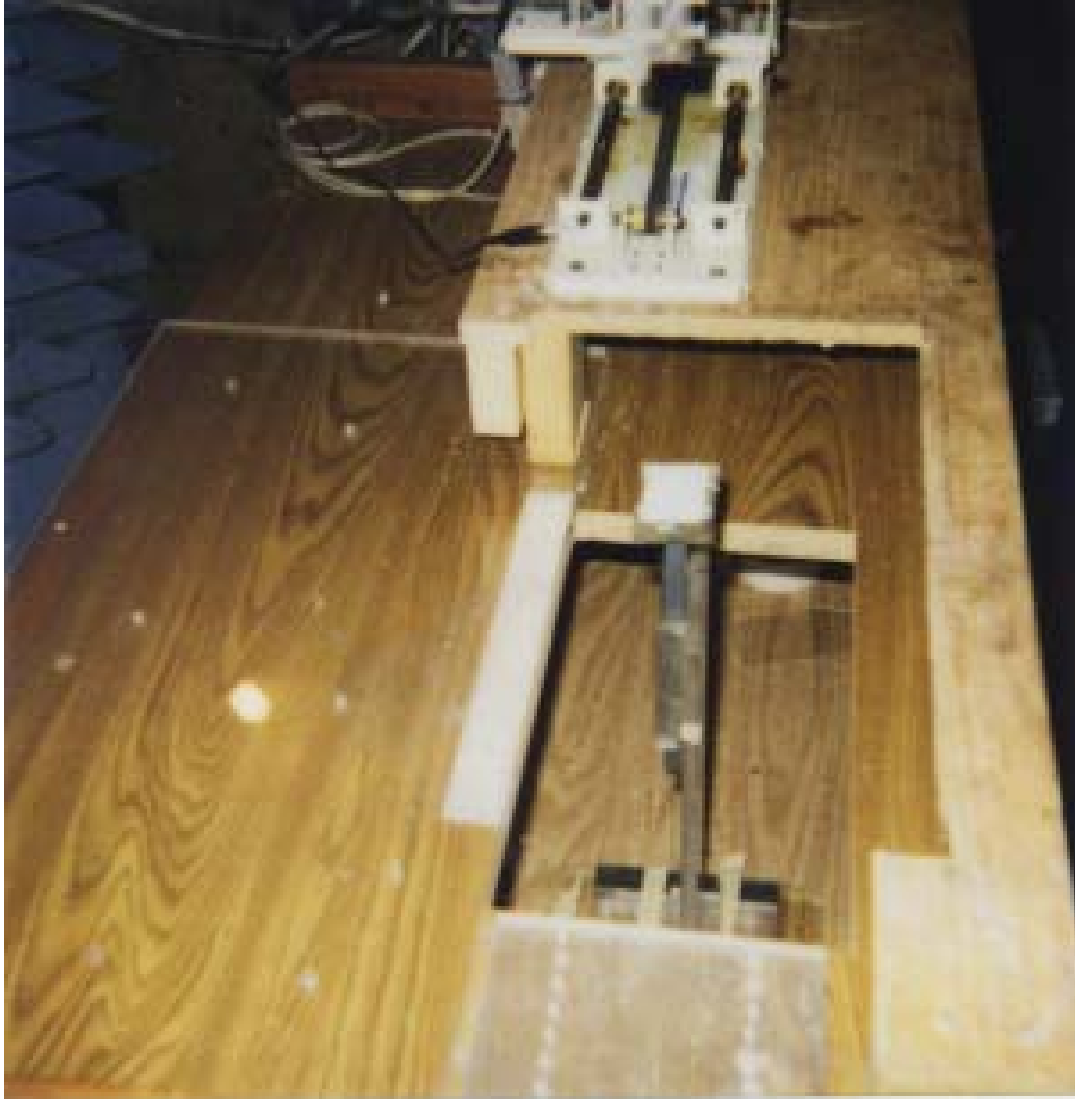
Fig. 6.   The plastic holder used to support the portable PC with the D-Link Model DWL-AG650 Cardbus Adapter (shown in Fig. 1).
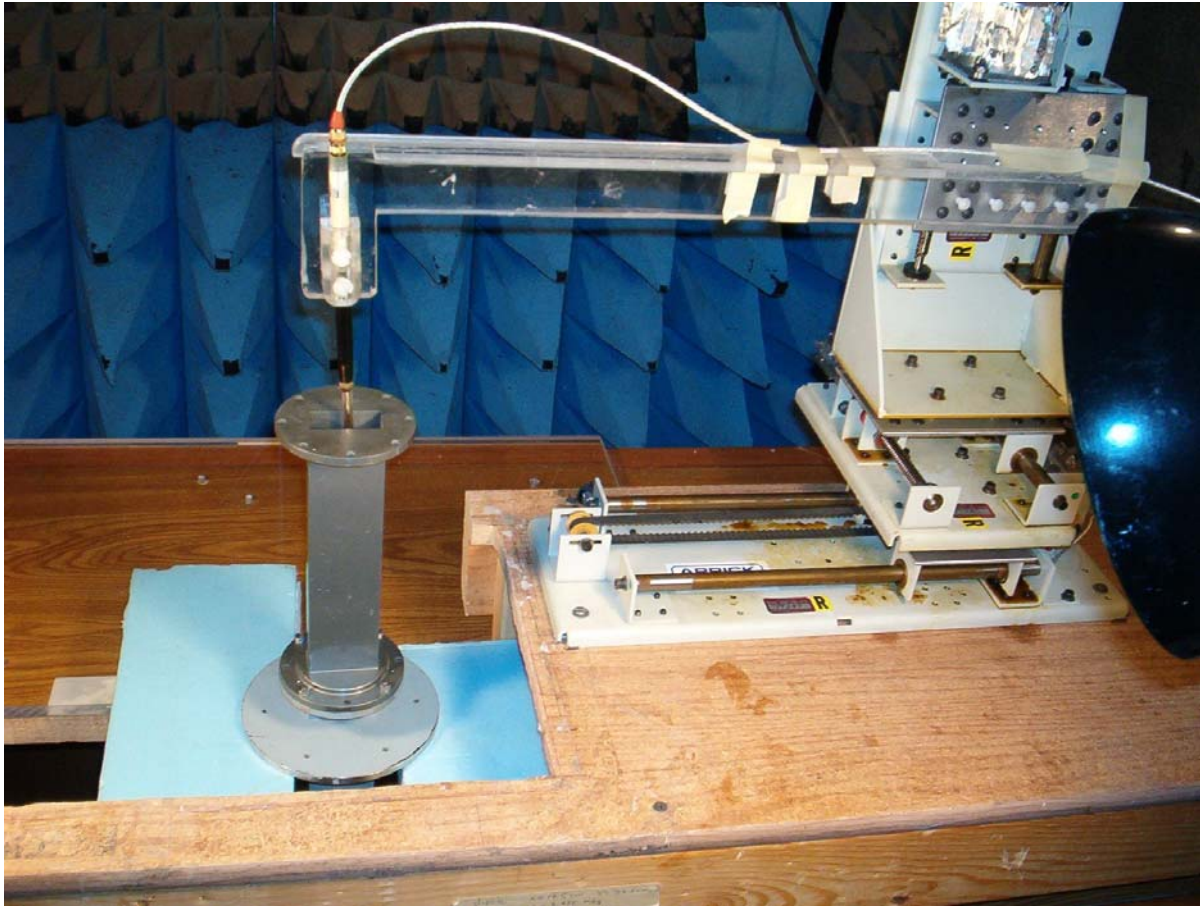
Fig. 7a.   A photograph of the waveguide setup used for calibration of the Narda Model 8021 E-field probe in the frequency band 5.2-5.8 GHz.
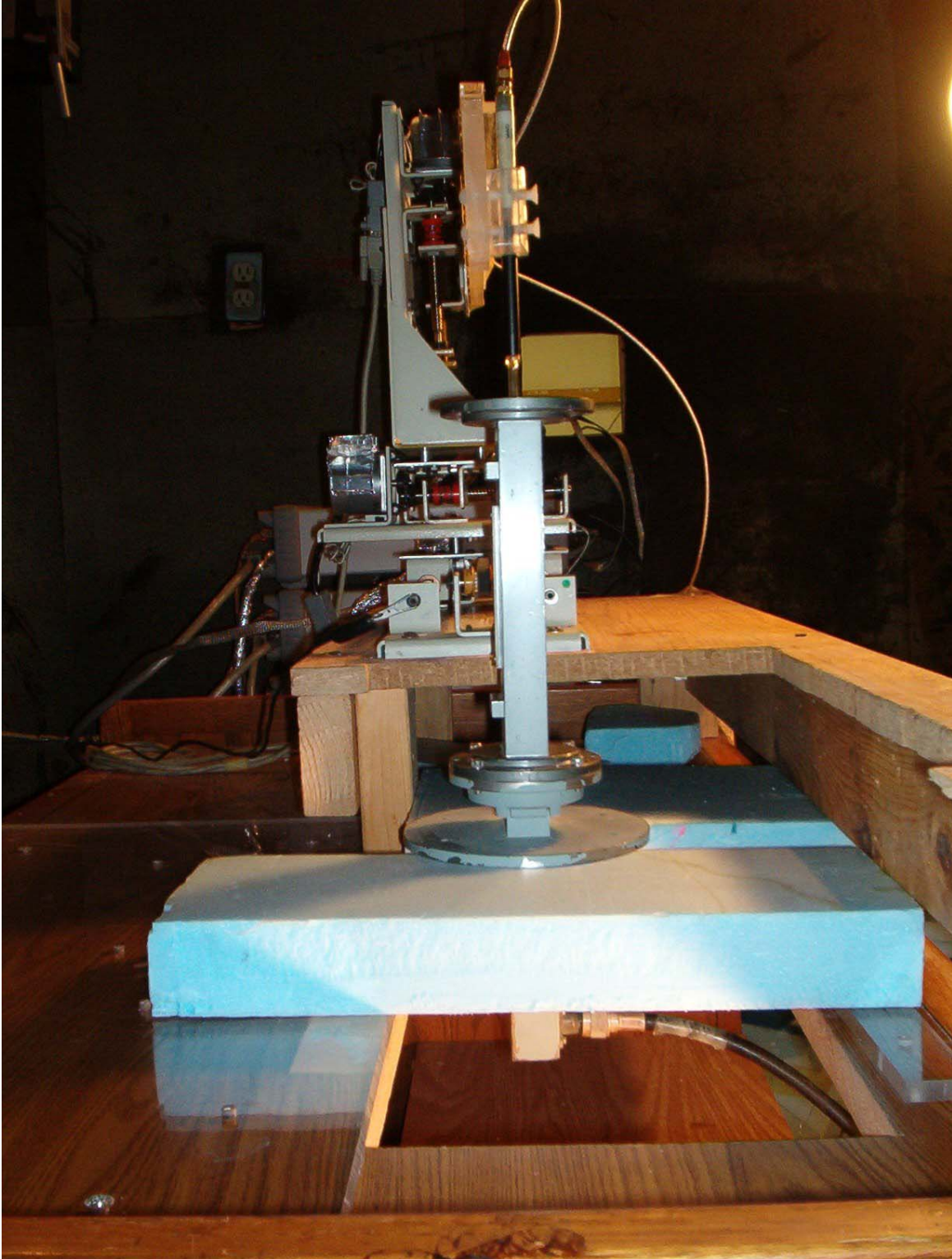
Fig. 7b.   Photograph of the waveguide setup showing also the coax to waveguide coupler at the bottom used to feed power to the vertical waveguide containing the tissue-simulant fluid.

Fig. 8.   Photograph of the Narda Model 8021 Broadband Electric Field
Probe used for SAR measurements.

Fig. 9.   Photograph of the half-wave dipole at 1900 MHz used for system verification.
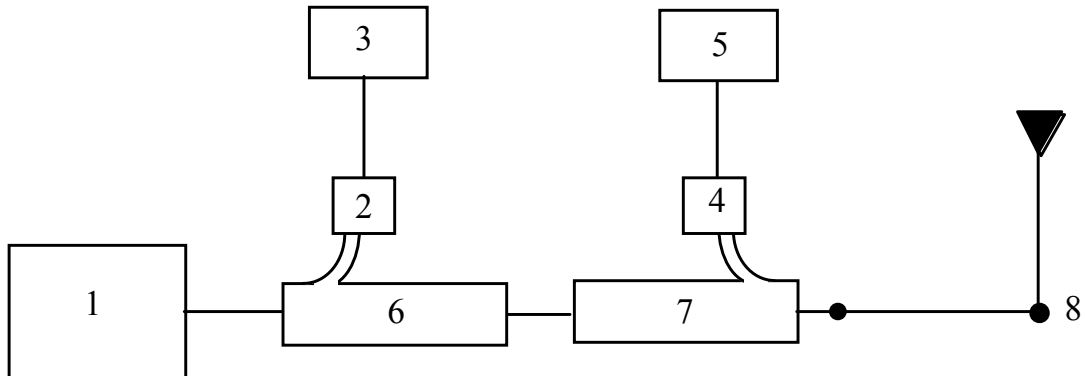
1. RF generator, MCL Model 15222 with Model 6051 plug-in (1000-2000 MHz).
2. HP Model 8481A power sensor.
3. HP Model 436A power meter.
4. HP Model 8482A power sensor.
5. HP Model 436A power meter.
6. Narda Model 3042B-30, 30 dB coaxial directional coupler.
7. Narda Model 3042-10, 10 dB coaxial directional coupler.
8. Reference dipole antenna.

Fig. 10.   The microwave circuit arrangement used for SAR system verification.

Fig. 11. Photograph of the Hewlett Packard Model 85070B Dielectric Probe. This is an open-circuited coaxial line probe.
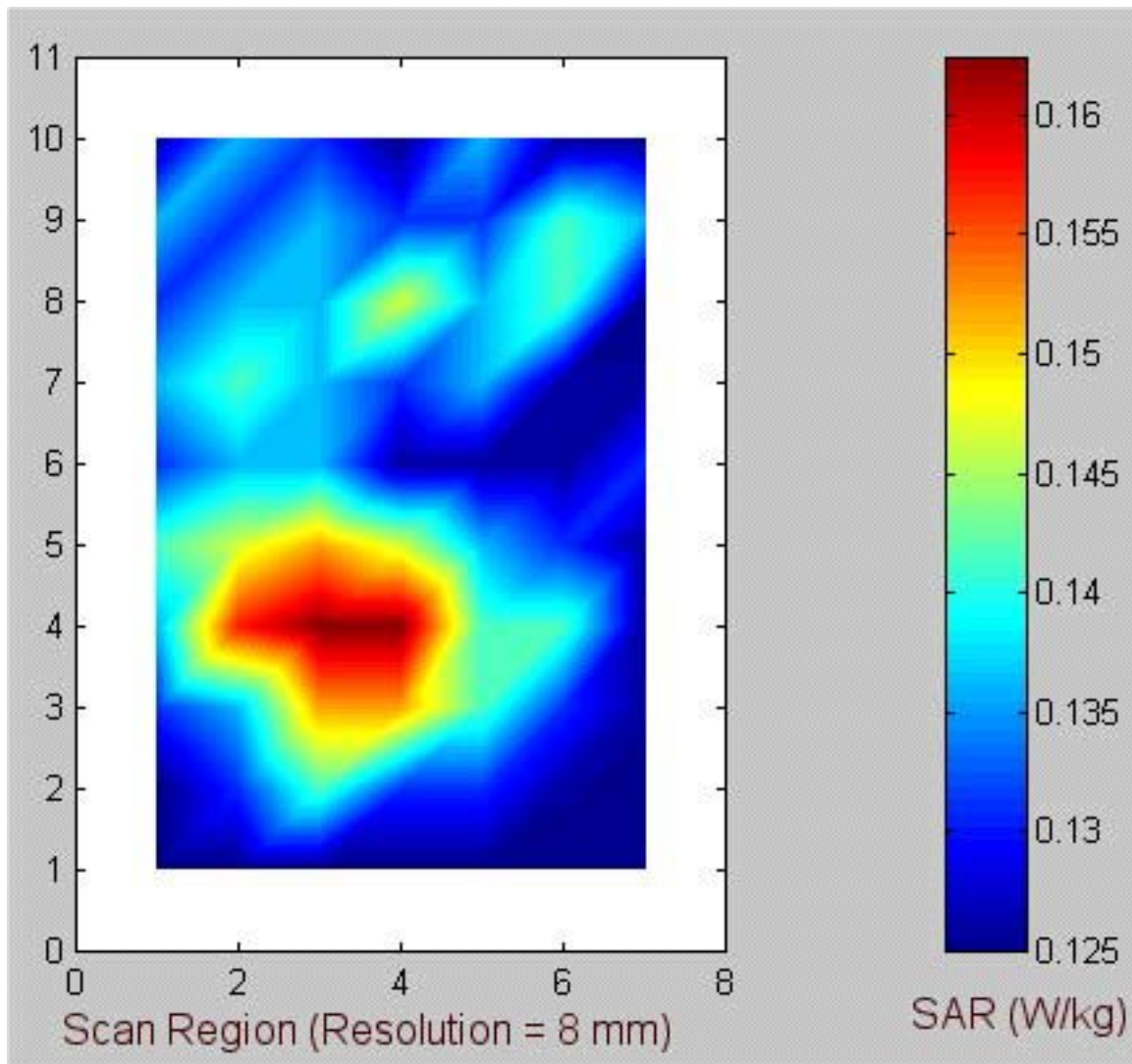
(a) 5.26 GHz normal mode (see Table 3 for the peak 1-g SAR).

Fig. 12.   Coarse scans for the SAR measurements for the **Above-lap position** of the PC relative to the flat phantom (Configuration 1, see Fig. 3).
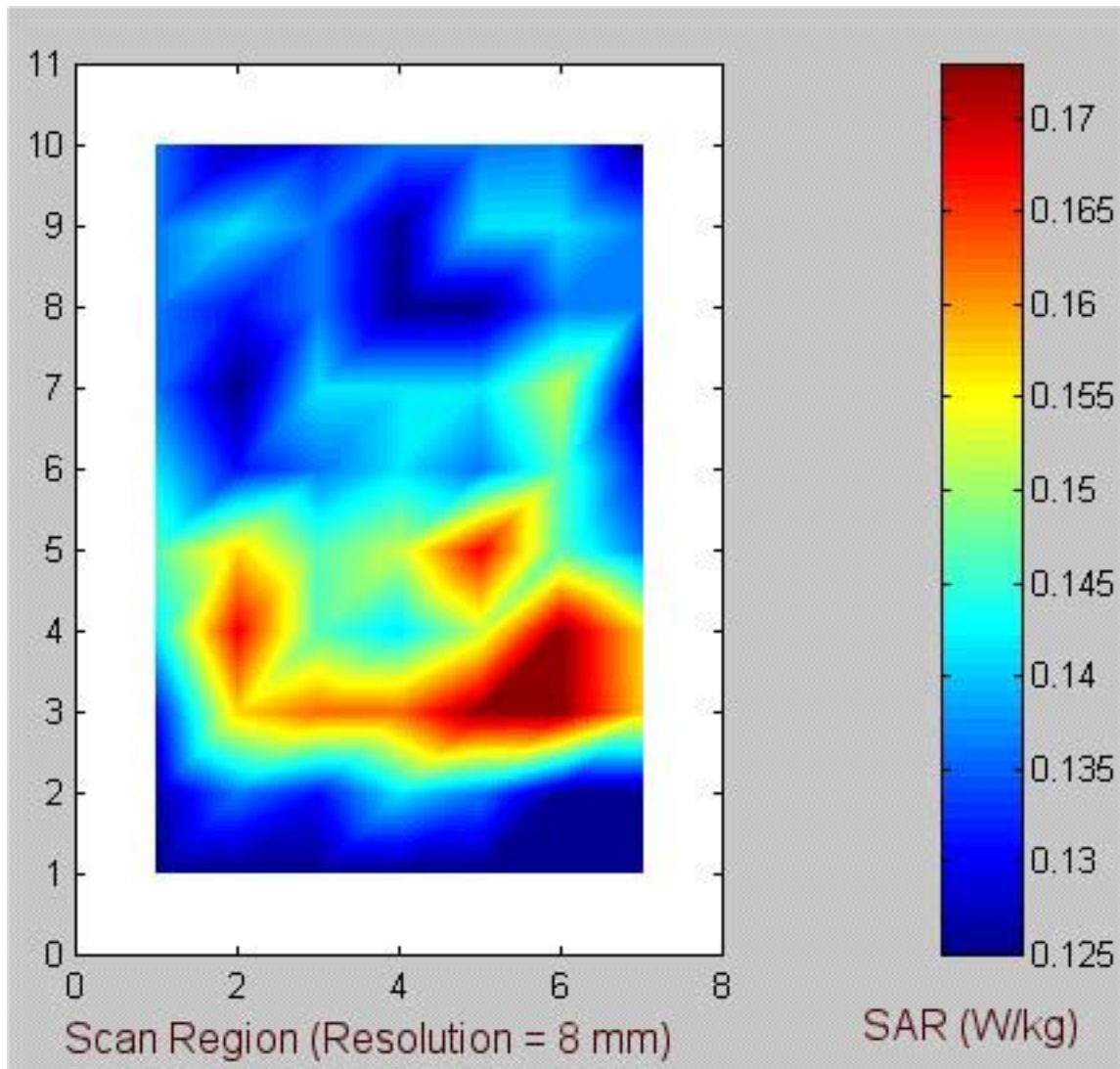
(b) 5.805 GHz normal mode (see Table 4 for the peak 1-g SAR).

Fig. 12.   Coarse scans for the SAR measurements for the **Above-lap position** of the PC relative to the flat phantom (Configuration 1, see Fig. 3).
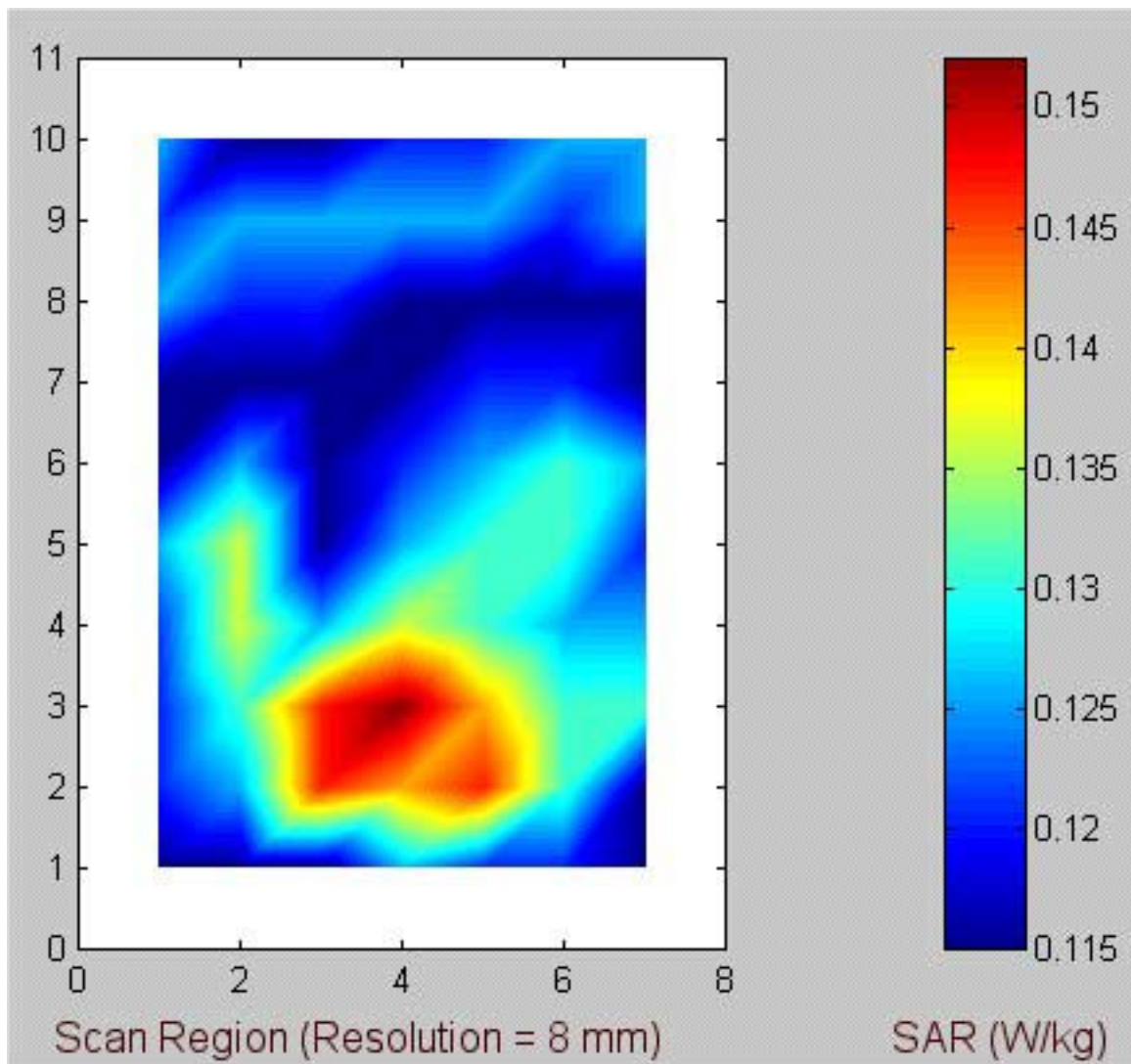
(a) 5.26 GHz normal mode (see Table 5 for the peak 1-g SAR).

Fig. 13. Coarse scans for the SAR measurements for the **Edge-on position** of the PC relative to the flat phantom (Configuration 2 – see Fig. 4). The PC was placed at 90° with the edge of the Cardbus Adapter pressed against the bottom of the flat phantom at a distance of 0 cm.
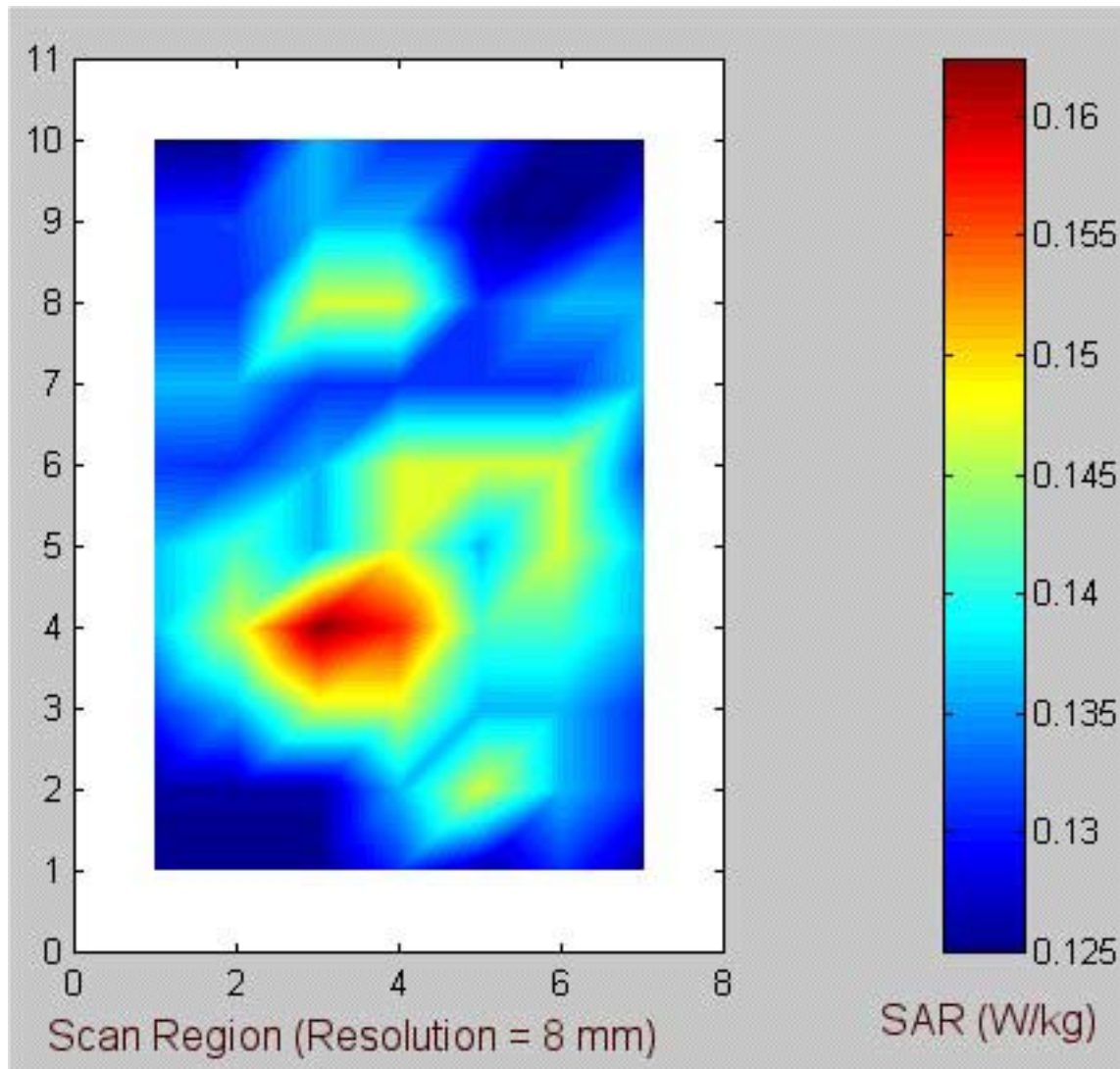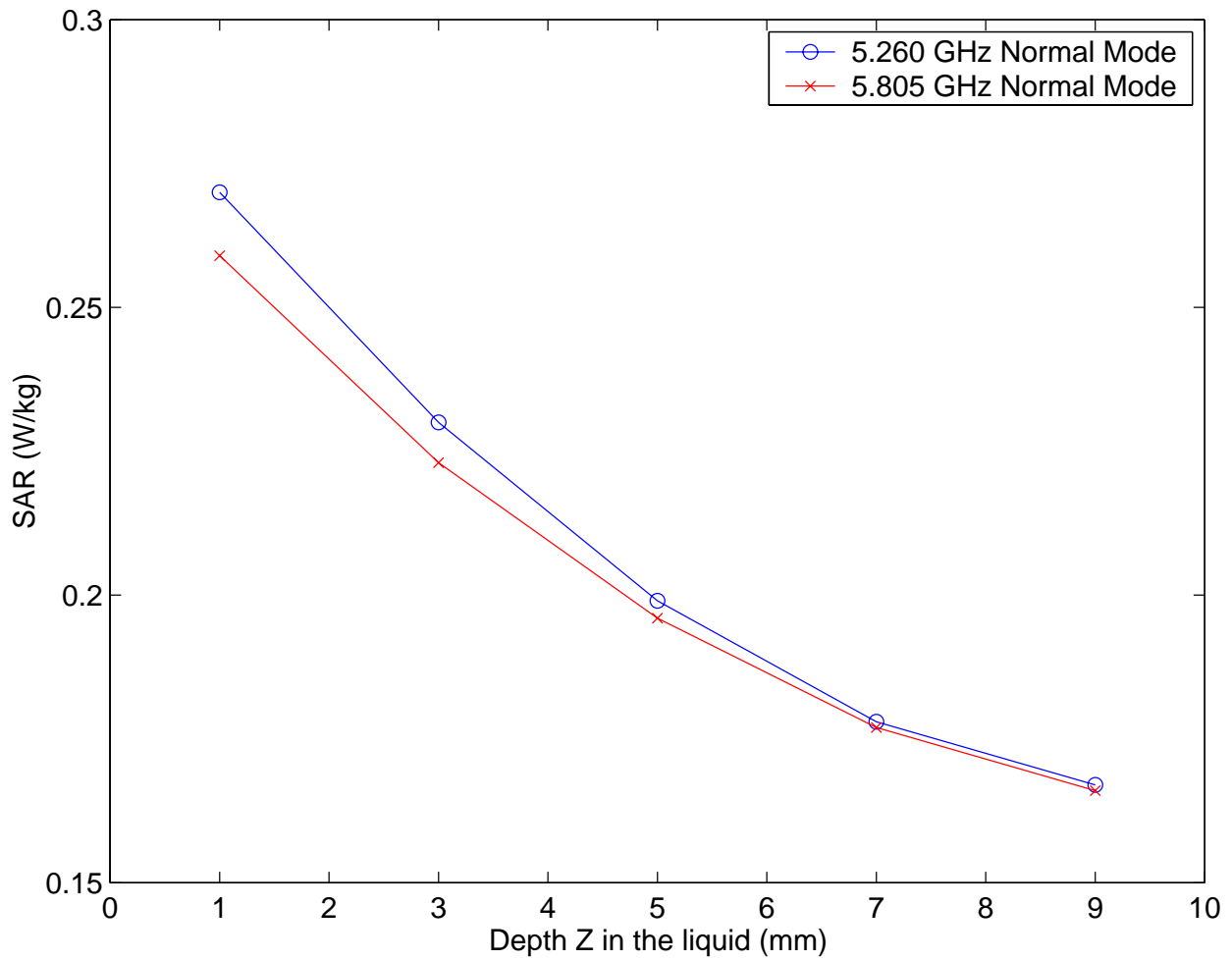
(b) 5.805 GHz normal mode (see Table 6 for the peak 1-g SAR).

Fig. 13.   Coarse scans for the SAR measurements for the **Edge-on position** of the PC relative to the flat phantom (Configuration 2 – see Fig. 4). The PC was placed at 90° with the edge of the Cardbus Adapter pressed against the bottom of the flat phantom at a distance of 0 cm.
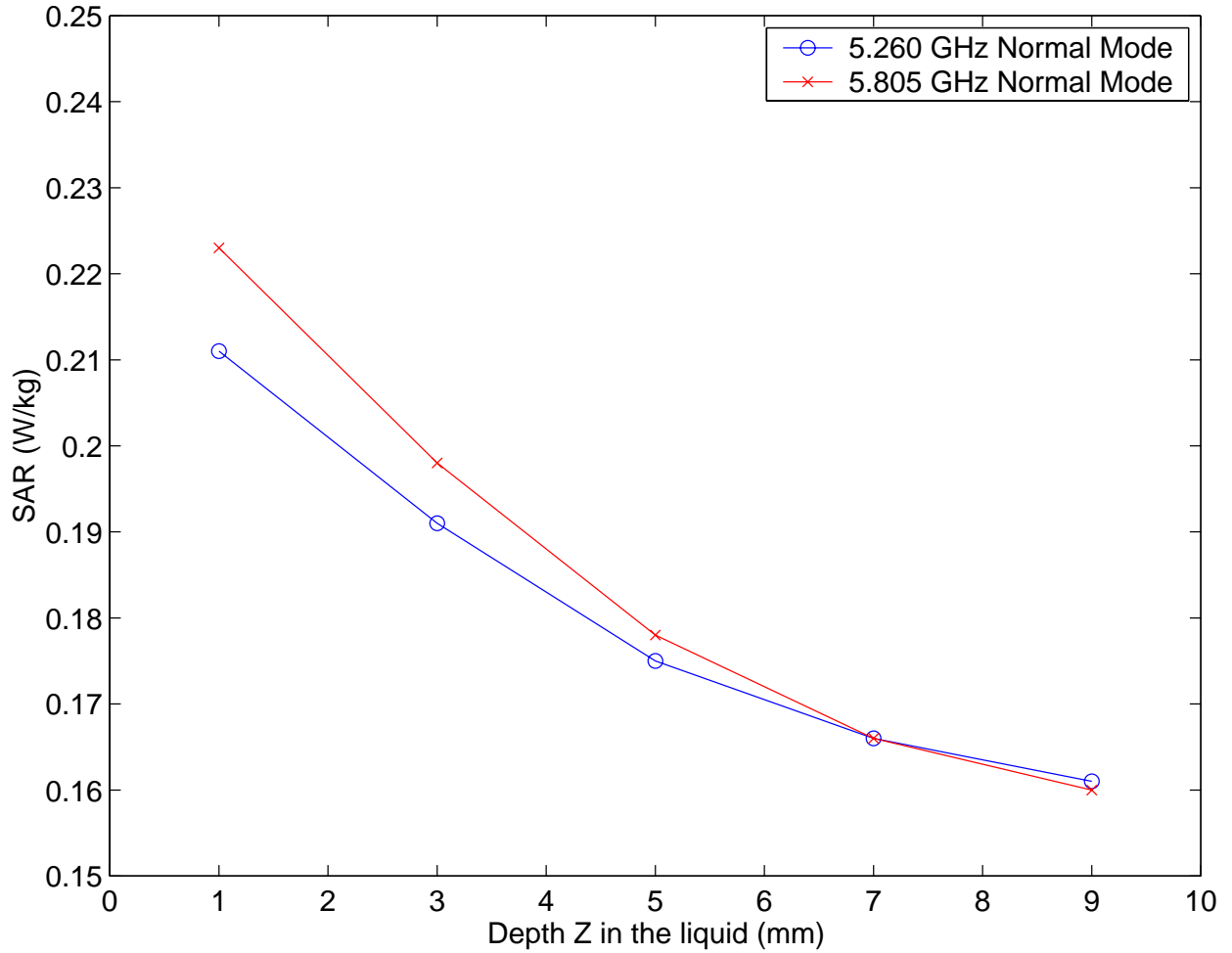
Fig. 14. Plot of the SAR variations as a function of depth Z in the liquid for locations of highest SAR (from Tables 3, 4 for **Above-lap position**) for D-Link Model DWL-AG650 Cardbus Adapter inserted into an IBM Model 2659 Laptop Computer.

Fig. 15. Plot of the SAR variations as a function of depth Z in the liquid for locations of highest SAR (from Tables 5, 6 for **Edge-on position**) for D-Link Model DWL-AG650 Cardbus Adapter inserted into an IBM Model 2659 Laptop Computer.

APPENDIX B

SAR System Verification for March 24, 2003

The measured SAR distribution for the peak 1-g SAR region using a dipole at 1900 MHz

For March 24, 2003 - The dipole SAR Plot
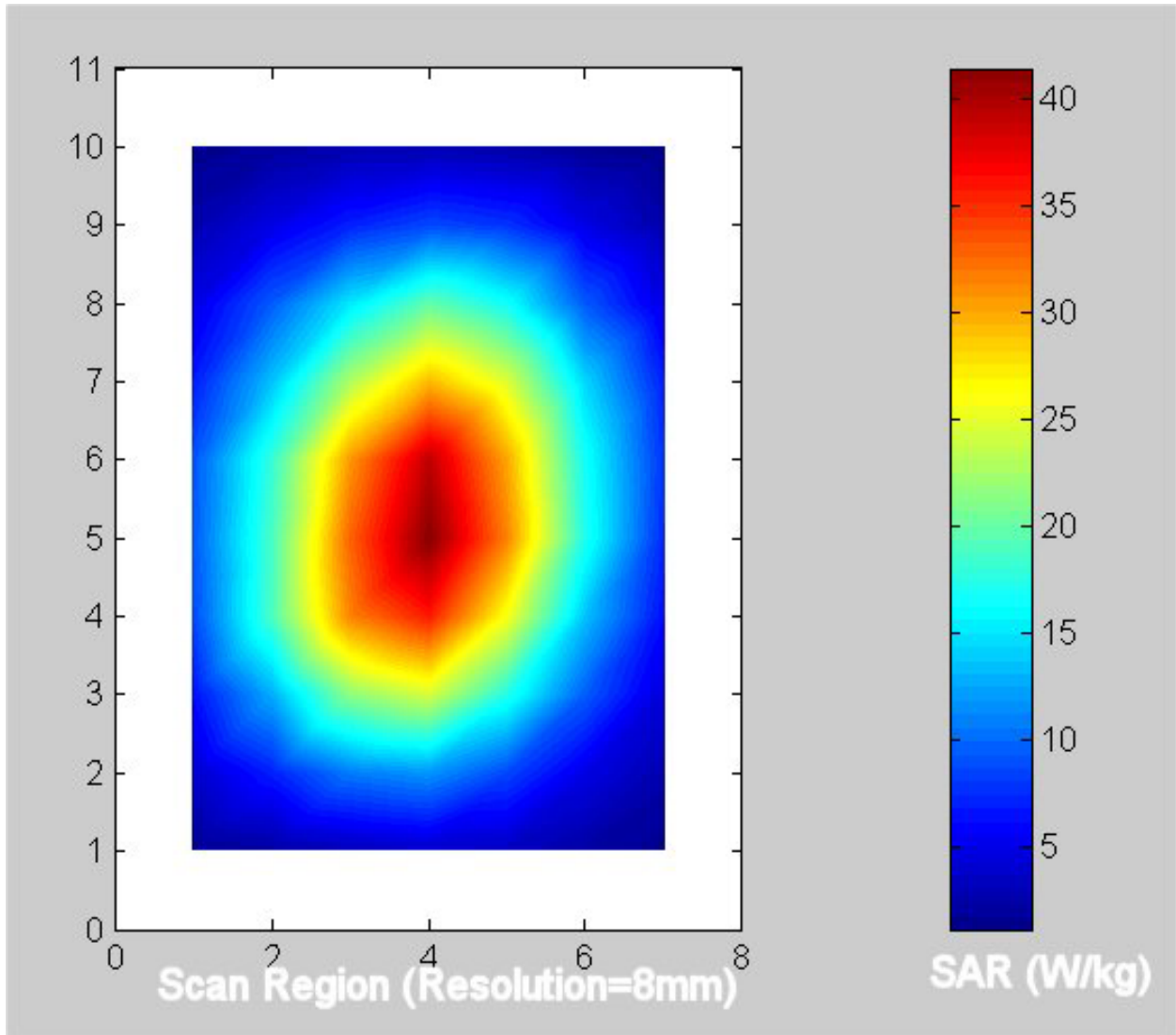
1-g SAR = 35.459 W/kg

a. At depth of 1 mm

55.333	56.340	54.485	55.908	51.891
54.956	59.826	56.400	56.916	51.890
57.769	59.093	58.283	54.792	54.149
59.060	59.880	57.873	58.097	52.526
57.622	59.379	56.586	56.832	51.069

b. At depth of 3 mm

43.200	44.000	42.872	43.344	40.192
43.185	45.966	44.080	44.157	40.699
44.775	46.085	45.268	43.009	42.161
45.615	46.458	45.226	44.844	41.474
44.625	46.079	44.602	44.408	40.419

c. At depth of 5 mm

33.025	33.629	33.066	32.836	30.461
33.254	34.514	33.707	33.518	31.282
33.953	35.151	34.384	33.074	32.119
34.438	35.238	34.558	33.818	32.062
33.794	34.943	34.418	33.915	31.349

d. At depth of 7 mm

24.807	25.225	25.066	24.387	22.700
25.164	25.470	25.282	24.999	23.640
25.303	26.292	25.632	24.988	24.022
25.529	26.220	25.868	25.018	24.289
25.130	25.971	26.033	25.354	23.860

e. At depth of 9 mm

18.546	18.789	18.874	17.995	16.907
18.915	18.834	18.805	18.598	17.772
18.825	19.506	19.011	18.750	17.872
18.887	19.406	19.158	18.444	18.155
18.632	19.162	19.447	18.725	17.952

Uncertainty Analysis

The uncertainty analysis of the University of Utah SAR Measurement System is given in Table A.1. Several of the numbers on tolerances are obtained by following procedures similar to those detailed in [8], while others have been obtained using methods suggested in [4].

Table B.1. Uncertainty analysis of the University of Utah SAR Measurement System.

Uncertainty Component	Tolerance ± %	Prob. Dist.	Div.	C_i 1-g	1-g u_i ± %
Measurement System					
Probe calibration	2.0	N	1	1	2.0
Axial istropy	4.0	R	$\sqrt{3}$	$(1-cp)^{1/2}$	1.6
Hemispherical isotropy	5.5	R	$\sqrt{3}$	$\sqrt{c_p}$	0.0
Boundary effect	0.8	R	$\sqrt{3}$	1	0.5
Linearity	3.0	R	$\sqrt{3}$	1	1.7
System detection limits	1.0	R	$\sqrt{3}$	1	0.6
Readout electronics	1.0	N	1	1	1.0
Response time	0.0	R	$\sqrt{3}$	1	0.0
Integration time	0.5	R	$\sqrt{3}$	1	0.3
RF ambient conditions	0	R	$\sqrt{3}$	1	0
Probe positioner mechanical tolerance	0.5	R	$\sqrt{3}$	1	0.3
Probe positioning with respect to phantom shell	2.0	R	$\sqrt{3}$	1	1.2
Extrapolation, interpolation, and integration algorithms for max. SAR evaluation	5.0	R	$\sqrt{3}$	1	2.9
Test Sample Related					
Test sample positioning	3	R	$\sqrt{3}$	1	1.7
Device holder uncertainty	3	R	$\sqrt{3}$	1	1.7
Output power variation - SAR drift measurement	5	R	$\sqrt{3}$	1	2.9
Phantom and Tissue Parameters					
Phantom uncertainty - shell thickness tolerance	10.0	R	$\sqrt{3}$	1	5.8
Liquid conductivity - deviation from target values	0.4	R	$\sqrt{3}$	0.7	0.2
Liquid conductivity - measurement uncertainty	1.5	R	$\sqrt{3}$	0.7	0.6
Liquid permitivity - deviation from target values	0.8	R	$\sqrt{3}$	0.6	0.3
Liquid permittivity - measurement uncertainty	3.5	R	$\sqrt{3}$	0.6	1.2
Combined Standard Uncertainty		RSS			8.3
Expanded Uncertainty (95% Confidence Level)					16.6

An Automated SAR Measurement System for Compliance Testing of Personal Wireless Devices

Qishan Yu, Om P. Gandhi, *Life Fellow, IEEE*, Magnus Aronsson, *Student Member, IEEE*, and Ding Wu

Abstract—An automated specific absorption rate (SAR) measurement system has been developed for compliance testing of personal wireless devices. Unlike other systems, this system uses a model with a lossy ear-shaped protrusion and the accuracy of this experimental setup has been checked by comparing the peak 1-g SAR's for ten cellular telephones, five each at 835 and 1900 MHz, with the results obtained using a 15-tissue anatomically based model with the finite-difference time-domain (FDTD) numerical electromagnetic technique. The SAR measurement system uses a three-dimensional (3-D) stepper motor to move a Narda Model 8021 E-field probe to measure the SAR distribution inside a head-shaped tissue-simulant phantom near the radiating device. The head and neck part of the model with an ear-shaped protrusion of 3 mm thickness is made of a lossy outer shell of 5–7 mm thickness of epoxy laced with KCl solution. The phantom is filled with appropriate frequency-specific fluids with measured electrical properties (dielectric constant and conductivity) that are close to the average for gray and white matters of the brain at the center frequencies of interest (835 and 1900 MHz). The implantable E-field probe is calibrated using the FDTD-calculated SAR variations for a slab model at two commonly used frequencies, 835 and 1900 MHz and is checked to have good isotropic characteristics (±0.23 dB) and a wide dynamic range (0.01–10 W/kg). The system is validated using a 223-mm-diameter sphere model. Peak 1-g SAR's for ten telephones using different antennas are within ±1 dB of those obtained using the FDTD numerical method for the anatomical model of the head and neck region.

Index Terms— Experimental phantom with lossy ear, safety compliance testing, validation against computed SAR.

I. INTRODUCTION

THE use of cellular telephones and mobile wireless communication systems has increased dramatically during the past few years. Meanwhile, there is public concern for safety of RF exposure from these devices. Since the RF exposure is quantified by the mass-normalized rate of electromagnetic energy absorption or the specific absorption rate (SAR), the United States Federal Communications Commission (FCC) requires that the SAR values of new personal wireless devices must meet the prescribed RF safety guidelines [1]. Furthermore, since electromagnetic energy absorbed by the human head depends to a large extent on the antenna used for the personal wireless devices [2], knowledge of SAR distributions in the human head can also help the industry to design better antennas to improve the performance of the wireless transceivers. In this regard, we should note that 30–65% of the power radiated by the whip antennas used today is wasted by absorption in the human head and hand [2] and this could be reduced greatly.

Recent dosimetric studies on the RF exposure to the human body from personal wireless devices have been carried out by both numerical simulation [3]–[5] and experimental measurements [6], [7]. Numerical methods using millimeter resolution anatomically based human body models and computer-aided design (CAD) files of cellular telephones can simulate the human body and the cellular phones in detail, respectively, thus providing highly accurate information about the electromagnetic coupling of the radiating device to the human body [8]. But the numerical technique requires considerable computational resources (memory and computation time) for just one test condition of the device. To alleviate this problem, use of the expanding grid finite-difference time-domain (FDTD) method [9] together with the use of the truncated models of the head [10] has resulted in savings of memory requirements by factors in excess of 20, making it possible to compute the high-resolution SAR distributions using workstations instead of parallel computers [8]. Nevertheless, if a device is to be tested for several orientations relative to the head or slightly variable conditions of the relatively unshielded internal circuitry, an easy, fast experimental procedure with validated accuracy and repeatability is of interest. A major requirement of the experimental setup, however, is that the phantom model be designed such that it gives peak 1-g SAR's that are in good agreement (within ±1 dB) with the values obtained using anatomically based models. While none of the previously developed thin shell phantoms can make this claim in this paper, we present an automated SAR measurement system that meets this requirement and can, therefore, be used for compliance testing at both 835 and 1900 MHz. The system is fully automated by a three-dimensional (3-D) stepper motor system controlled by a computer, with a miniature implantable E-field probe that is used to determine spatial SAR variations. Using an ear-shaped protrusion of 3 mm thickness, the head and neck part of the phantom model is made of a lossy shell of 5–7 mm thickness of epoxy laced with KCl solution to simulate the thickness of the human skull. This is important since most of the electromagnetic energy absorption for the region of the highest SAR for anatomically based models occurs either for the ear or the internal tissues beyond the skull, which is on the order of 5–7 mm thick. This and the upper part of the torso are filled with a frequency specific fluid with measured electrical properties (dielectric constant and conductivity) close to the average properties of the brain
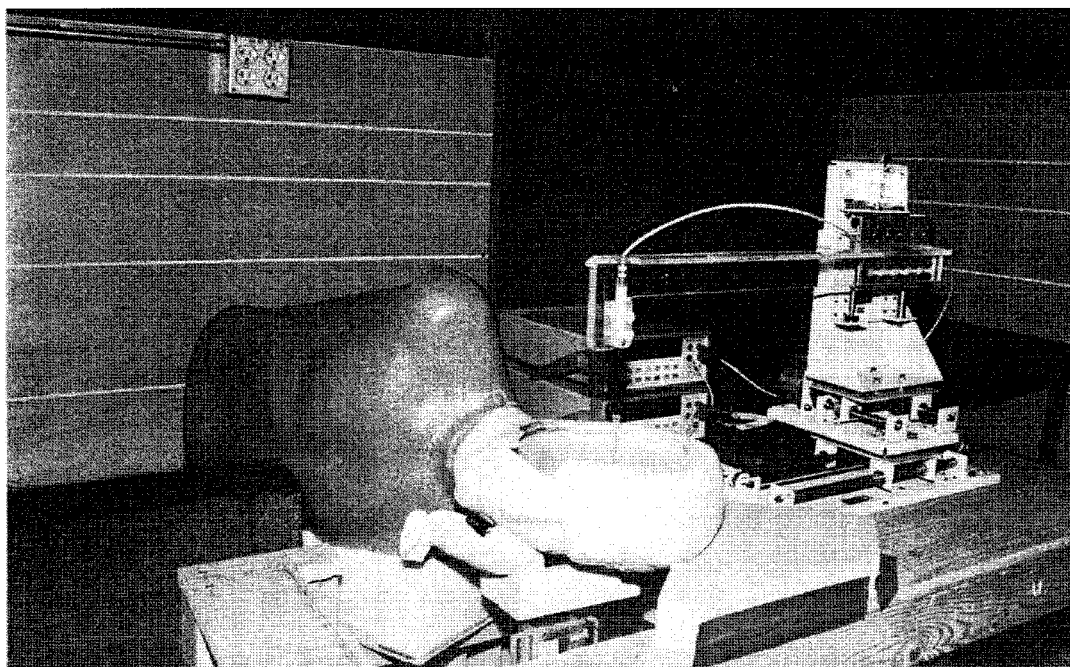
Fig. 1. Phantom model used in the automated SAR measurement system.

for white and gray matters at the center frequency of interest. Ten cellular telephones—five each at 835 and 1900 MHz with different types of antennas—have been measured for peak 1-g SAR's using this system. As desired, agreement with the FDTD calculated 1-g SAR's using an anatomically based model of a male adult is within ±1 dB.

II. EXPERIMENTAL SETUP AND MEASUREMENTS

A. Experimental Setup

A photograph of the phantom model together with the computer controlled 3-D stepper motor system (Arrick Robotics MD-2A) is shown in Fig. 1. A triaxial Narda Model 8021 E-field probe is used to determine the internal electric fields. The positioning repeatability of the stepper motor system moving the E-field probe is within ±0.1 mm. Outputs from the three channels of the E-field probe are dc voltages, the sum of which is proportional to the square of the internal electric fields ($|E_i|^2$) from which the SAR can be obtained from the equation SAR $= \sigma(|E_i|^2)/\rho$, where σ and ρ are the conductivity and mass density of the tissue-simulant material, respectively [11]. The dc voltages for the three channels of the E-field probe are read by three HP 34401A multimeters and sent to the computer via an HPIB interface. The setup is carefully grounded and shielded to reduce the noise due to the electromagnetic interference (EMI).

The topography of the internal surface of the phantom is prescanned with a high resolution of 2 mm × 2 mm so that the computer knows how far it can move the probe in the vertical direction (y) at each horizontal position (x, z) without breaking the probe. For scanning of the contours of the internal surface, a thin copper tape is applied to the internal surface of the phantom. Then a metal rod with the same shape and diameter as the E-field probe is moved by the stepper motor

TABLE I
DESIRED TISSUE PROPERTIES AND THE MEASURED ELECTRICAL PROPERTIES OF
THE TISSUE-SIMULANT MATERIALS FOR THE PHANTOM MODEL

	Desired[*]		Measured	
	ε_r	σ (S/m)	ε_r	σ (S/m)
		835 MHz		
Brain	45.3	0.92	41.1 ± 1.4	1.06 ± 0.05
Skull	17.4	0.25	7.4	0.16
		1900 MHz		
Brain	43.2	1.29	45.5 ± 1.7	1.31 ± 0.06
Skull	16.4	0.45	7.4	0.34

*From C. Gabriel [12]

system on a programmed path to detect the surface area of dimensions 4.8 cm × 14.4 cm including the region of the ear and above the ear and the region of the cheek since various devices result in the highest SAR's for any of these regions. When the metal rod's tip touches the surface, an electrical signal is sent to the computer, the computer stops the stepper motor and records the position (x, y, z). Since the positions of the stepper motor system and the phantom are relatively stable, prescanning of the phantom surface is needed only once for either the right-eared or the left-eared phantom model.

The compliance testing procedure consists of two steps. A coarser sampling with a step size of 8 mm is done in the first instance to locate the peak SAR region. The peak SAR region is then sampled with a finer step size of 2 mm on a 3-D grid over a 1 cm^3 volume cube, i.e., a total of 5 × 5 × 5 points. Since the dipole sensors of the Narda Model

TABLE II
COMPOSITION USED FOR BRAIN EQUIVALENT MATERIALS

835 MHz		1900 MHz	
Water	40.4%	Water	60.0%
Sugar	56.0%	Sugar	18.0%
Salt (NaCl)	2.5%	PEP	20.0%
HEC	1.0%	Salt (NaCl)	0.4%
		TX 151	1.6%
$\varepsilon_r = 41.1 \pm 1.4$		$\varepsilon_r = 45.5 \pm 1.7$	
$\sigma = 1.06 \pm 0.05$ S/m		$\sigma = 1.31 \pm 0.06$ S/m	

TABLE III
LONG-TERM STABILITY OF THE PHANTOM MATERIAL AT 1900 MHz

Day	ε_r	σ (S/m)
1	46.2 ± 1.1	1.35 ± 0.03
7	44.9 ± 1.7	1.29 ± 0.06
15	44.2 ± 1.8	1.25 ± 0.05

8021 E-field probe are recessed about 4 mm from the tip of the probe, it is necessary to use an extrapolation subroutine to extend the SAR's measured in depth (y) for each of the (x, z) positions to the internal surface of the phantom $(y = 0)$ as these SAR's are generally the highest and contribute the most to the peak 1-g SAR's. We have found that a second-order polynomial obtained by using the least mean square error method is adequate and, as can be seen from the data given in Tables IV and V, gives peak 1-g SAR's that are generally within $\pm 10\%$ of the FDTD calculated results. The whole testing procedure takes about 20 min with coarser and finer sampling steps taking about 10 min each, so the measurement can be finished within the battery charge life of most personal wireless devices.

B. Phantom Model

The phantom model is shown in Fig. 1. The head of the phantom model has an axial length of 26 cm from the chin to the top of the head; the distance from location of the ear canal to top of the head is 14.7 cm and the width from side to side is 16.5 cm. These dimensions are typical for adult human beings. Similar to the thickness of the human skull, the head and neck part of the model is made of an outer shell of 5–7 mm thickness of epoxy laced with KCl solution for losses, except that the protruding ear region is somewhat thinner and only about 3 mm thick and this region is filled with lossy tissue-simulant material. In this regard, this phantom model is different from the thin shell models using either lossless solid plastic ears or equivalent spacers that have been used in the past [6], [7]. This and the upper part of the torso are filled with appropriate frequency-specific fluids with measured electrical properties (dielectric constant and conductivity) close to the average properties of the brain for white and gray matters at the center frequencies of interest. Table I shows the desired tissue properties [12] and the measured electrical properties of the skull-and brain-simulant materials at 835 and 1900 MHz. The head and neck region of the phantom is filled with brain simulating fluids of compositions given in Table II. A semi-solid composition of water, salt, polyethylene powder, and a gelling agent TX151 that simulates the dielectric properties equivalent to those of two-thirds muscle is used to fill a thin surgical rubber glove to create the shape of the hand. As

shown in Fig. 1, the "hand" thus created is used to hold the cellular telephone, which is positioned against the phantom head along the line connecting the ear canal and the mouth of the phantom. This is done in order to load the handset similar to the dielectric loading provided by the hand in actual use of a hand-held wireless device.

Two different fluids of compositions given in Table II are used to simulate the average dielectric properties of the brain at 835 and 1900 MHz. The clear fluid used at 835 MHz is a composition of water, sugar, salt, and a gelling agent HEC proposed by Hartsgrave *et al.* [13]. Even without salt, this composition has an electrical conductivity $\sigma = 1.65$ S/m, which is considerably higher than $\sigma = 1.29$ S/m needed to simulate the average properties for the gray and white matters of the brain at 1900 MHz [12]. Thus, we have developed another liquid brain simulating material for SAR measurements at 1900 MHz. The composition of this material is also given in Table II. The dielectric properties of this material were measured using a HP 85070B dielectric probe measurement system and are given in Table II. The brain-simulant composition for use at 1900 MHz has shown a very good long-term stability (Table III) when it is properly sealed after each of the measurements to minimize the evaporation of water.
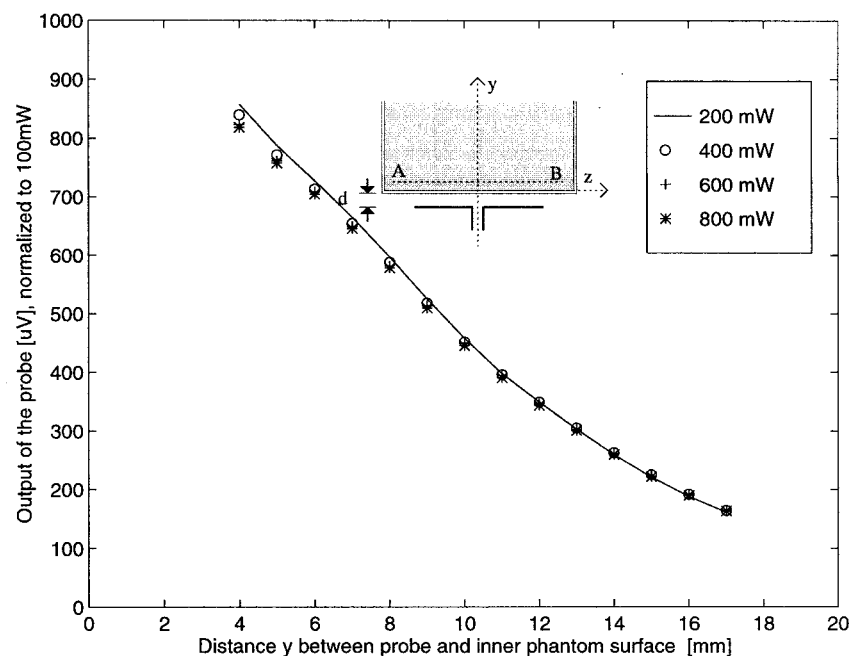
C. E-Field Probe

The nonperturbing implantable E-field probe used in the setup was originally developed by Bassen *et al.* [14] and is now manufactured by L3/Narda Microwave Corporation, Hauppauge, NY as Model 8021 E-field probe. In the probe, three orthogonal miniature dipoles are placed on a triangular-beam substrate. Each dipole is loaded with a small Schottky diode and connected to the external circuitry by high resistance (2 MΩ $\pm 40\%$) leads to reduce secondary pickups. The entire structure is then encapsulated with a low dielectric constant insulating material. The probe thus constructed has a very small diameter (4 mm), which results in a relatively small perturbation of the internal electric field.

1) Test for Square-Law Region: It is necessary to operate the E-field probe in the square-law region for each of the diodes so that the sum of the dc voltage outputs from the three dipoles is proportional to the square of the internal electric field $(|E_i|^2)$. Fortunately, the personal wireless devices induce SAR's that are generally less than 5–6 W/kg even for closest locations of the head [2]. For compliance testing it is therefore
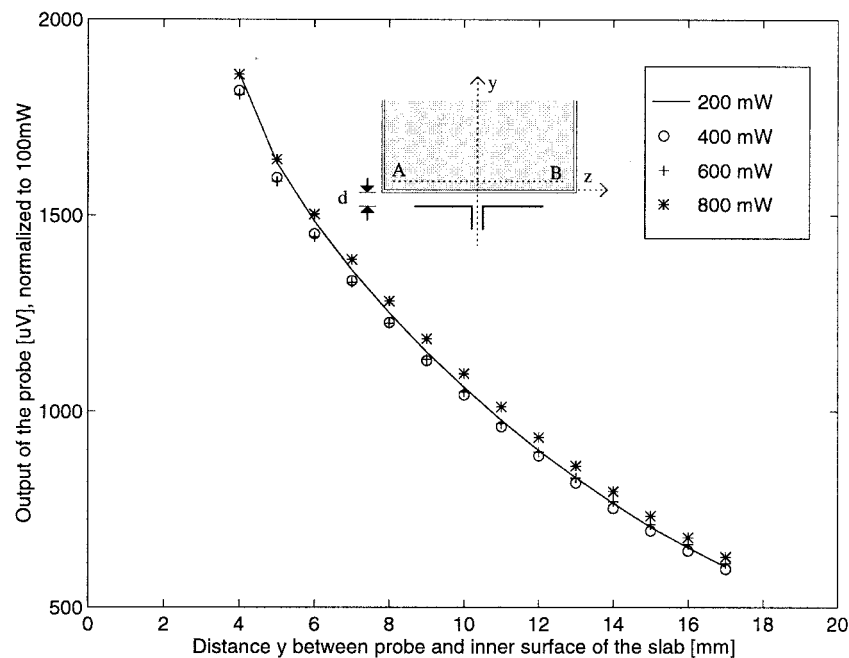
(a)

(b)

Fig. 2. Variation of the output voltage (proportional to $|E_i|^2$) for different radiated powers normalized to 0.1 W. (a) Test for square-law behavior at 835 MHz. (b) Test for square-law behavior at 1900 MHz.

necessary that the E-field probe be checked for square-law behavior for SAR's up to such values that are likely to be encountered. Such a test may be conducted using a canonical lossy body, e.g, a rectangular box or a sphere irradiated by a dipole. By varying the radiated power of the dipole, the output of the probe should increase linearly with the applied power for each of the test locations.

Shown in Fig. 2(a) and (b) are the results of the tests performed to check the square-law behavior of the E-field

probe used in our setup at 835 and 1900 MHz, respectively. For these measurements we have used a rectangular box of external dimensions 30 × 15.5 × 50 cm that was irradiated by the corresponding half-wave dipoles with different amounts of radiated powers from 200–800 mW. This box of thickness 0.635 cm was filled to a depth of 13 cm with corresponding brain-simulant fluids (Table II). Used for radiators were nominal half-wave length dipoles of lengths 178 and 77 mm at 835 and 1900 MHz, respectively. Since the dc voltage outputs
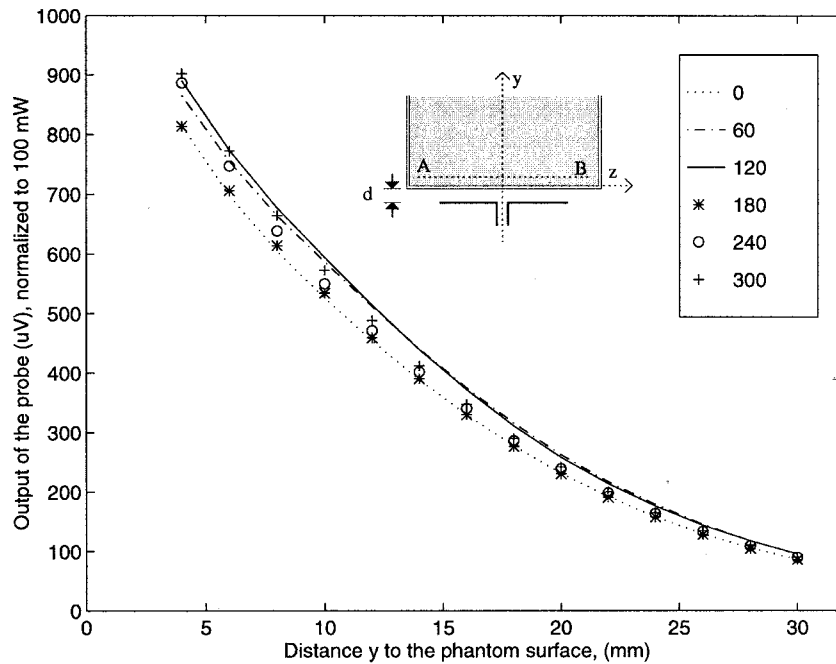
(a)
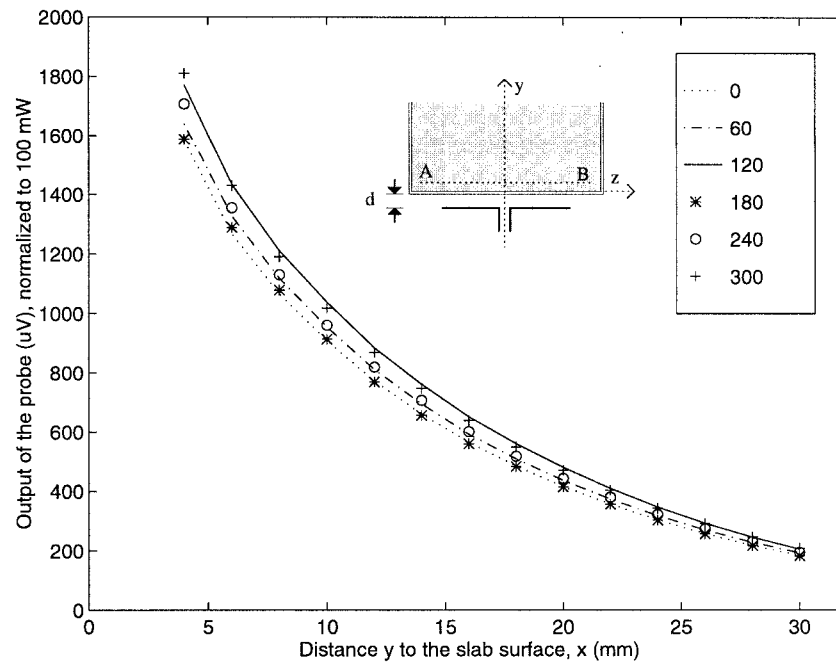
(b)

Fig. 3. (a) Test for isotropy at 835 MHz. (b) Test for isotropy at 1900 MHz.

of the probe are fairly similar when normalized to a radiated power of 100 mW, the square-law behavior is demonstrated and an output voltage that is proportional to $|E_i|^2$ is obtained within ±3%.

2) Test for Isotropy of the Probe: Another important characteristic of the probe that affects the measurement accuracy is its isotropy. Since the orientation of the induced electric field is generally unknown, the E-field probe should be relatively isotropic in its response to the orientation of the E-field. Shown in Fig. 3(a) and (b) are the test results of the E-field

probe used in our setup at 835 and 1900 MHz, respectively. The previously described box phantom of thickness 0.635 cm and external dimensions 30 × 15.5 × 50 cm along x, y, and z dimensions, respectively, was used for these measurements. Also used for these measurements were the two half-wavelength dipoles described above at 835 and 1900 MHz, respectively. The E-field probe was rotated around its axis from 0–360° in incremental steps of 60°. As seen in Fig. 3(a) and (b), an isotropy of less than ±0.23 dB (±5.5%) was observed for this E-field probe both at 835 and 1900 MHz.
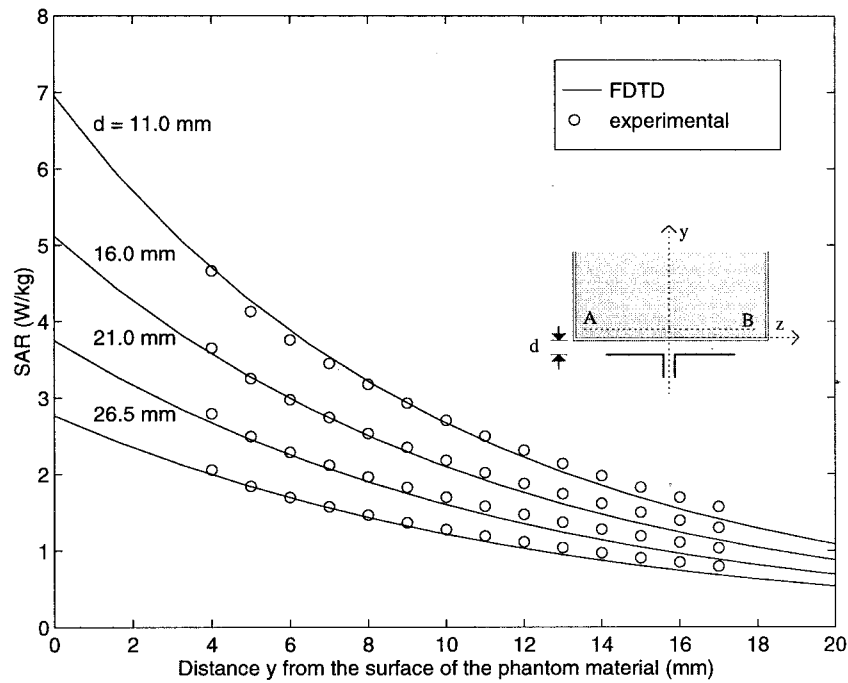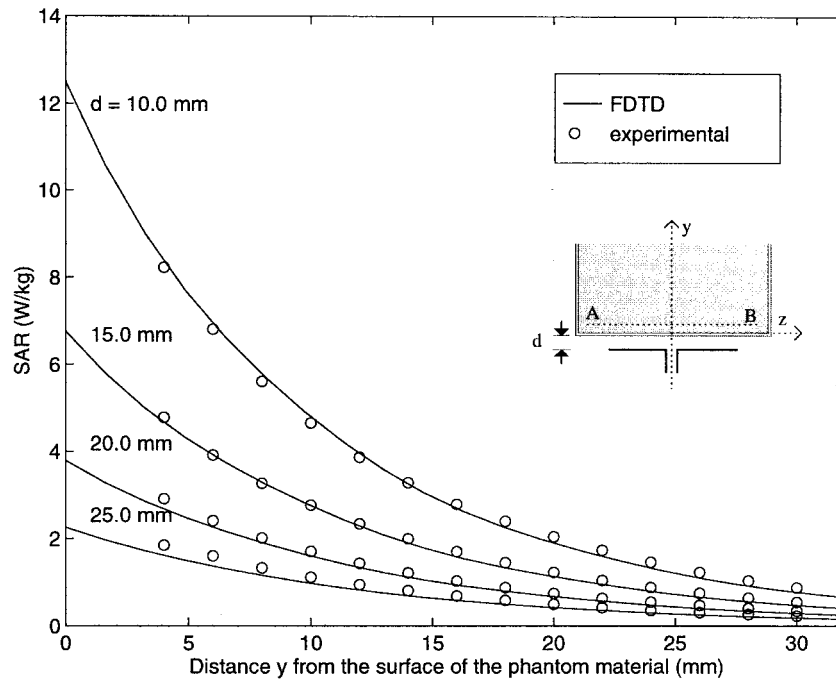
(a)
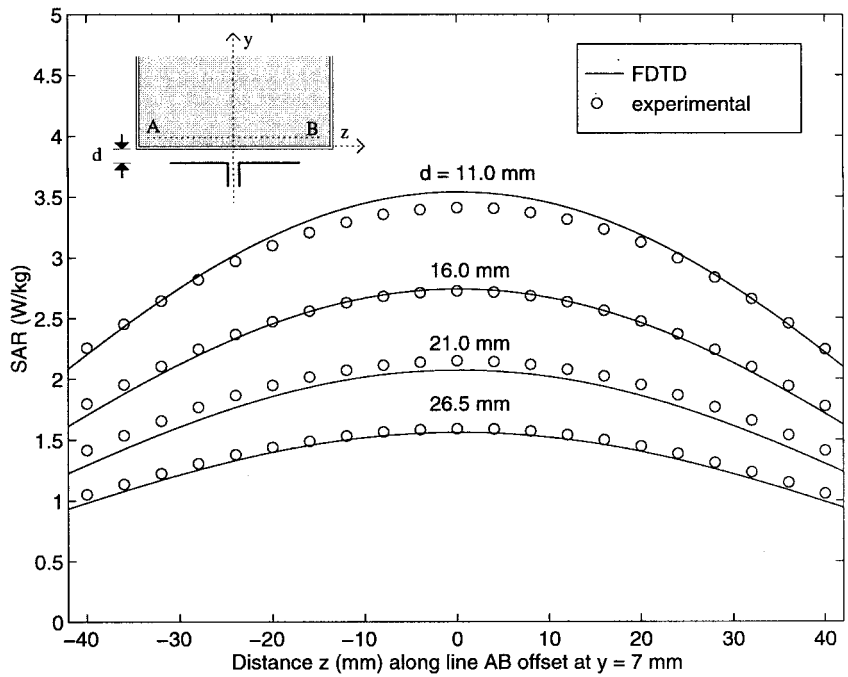
(b)

Fig. 4. Comparison of the calculated and measured SAR variations for a box phantom of external dimensions $30 \times 15.5 \times 50$ cm; 835 MHz; $\lambda/2$ dipole antenna; 0.5-W radiated power. Calibration factor for the Narda Model 8021 probe at 835 MHz $= 0.39$ (mW/kg)/μV. Measured for the phantom material $\varepsilon_r = 41.1$, $\sigma = 1.06$ S/m. (a) Variation of SAR along the y axis. (b) For a line AB parallel to the z axis at a distance $y = 7$ mm from the surface of the phantom material.

3) Calibration of the E-Field Probe: Since the voltage output of the E-field probe is proportional to the square of the internal electric field ($|E_i|^2$), the SAR is, therefore, proportional to the voltage output of the E-field probe by a proportionality constant C. The constant C is defined as the calibration factor and is frequency and material dependent. It is measured to calibrate the probe at the various frequencies of

interest using the appropriate tissue-simulating materials for the respective frequencies.

Canonical geometries such as waveguides, rectangular slabs, and layered or homogeneous spheres have, in the past, been used for the calibration of the implantable E-field probe [15]–[17]. Since the FDTD method has been carefully validated to solve electromagnetic problems for a variety of

(a)
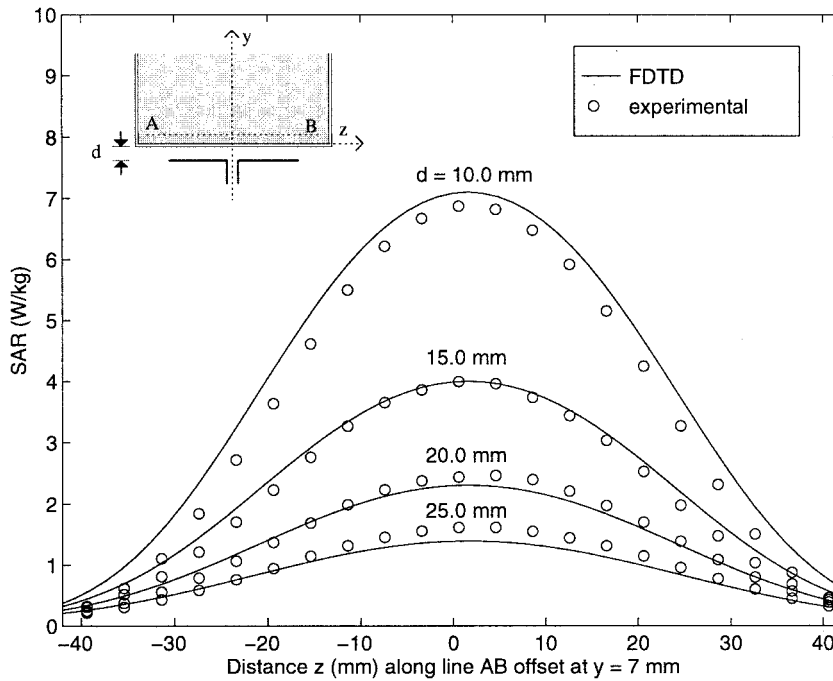
(b)

Fig. 5.   Comparison of the calculated and measured SAR variations for a box phantom of external dimensions 30 × 15.5 × 50 cm; 1900 MHz; $\lambda/2$ dipole antenna; 0.5 W radiated power. Calibration factor for the Narda Model 8021 probe at 1900 MHz = 0.565 (mW/kg)/μV. Measured for the phantom material. (a) Variation of SAR along the y axis. (b) For a line AB parallel to the z axis at a distance $y = 7$ mm from the surface of the phantom material.

geometries [18], [19], we were able to calibrate the Narda E-field probe by comparing the measured variations of the probe voltage ($\propto |E_i|^2$) against the FDTD calculated variations of SAR's for a box phantom of external dimensions 30 × 15.5 × 50 cm used previously for the data given in Figs. 2 and 3, respectively. For these measurements, we placed the nominal half-wave dipoles of lengths 178 and 77 mm at 835 and

1900 MHz, respectively, at several distances d [see inserts of Figs. 4(a), (b) and 5(a), (b)] from the outer surface of the acrylic, ($\varepsilon_r = 2.56$) box of thickness 6.35 mm. Shown in Figs. 4(a) and (b) and 5(a) and (b) are the comparisons between the experimentally measured and FDTD-calculated variations of the SAR distributions in the tissue-simulant fluid for this box phantom made of an acrylic base and sides. Since
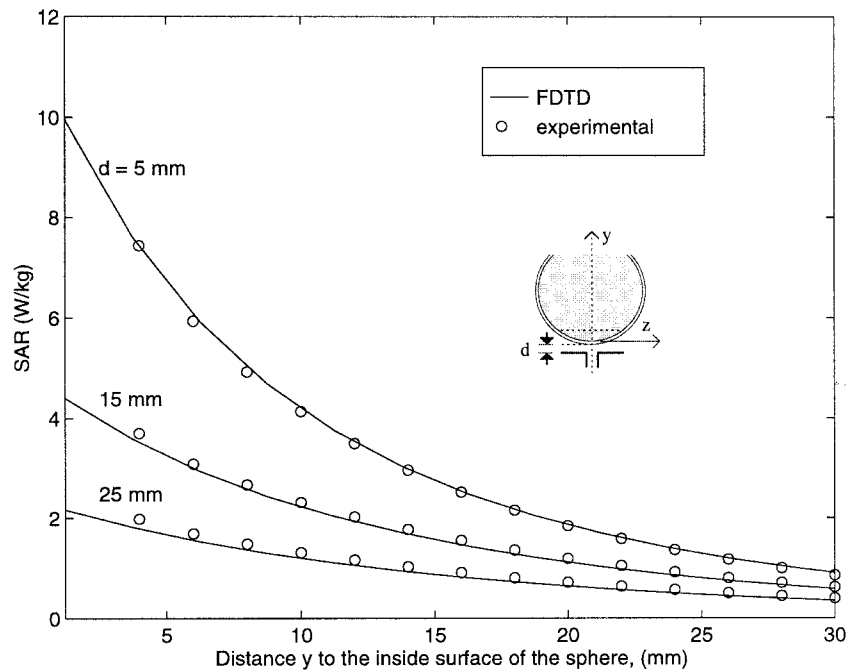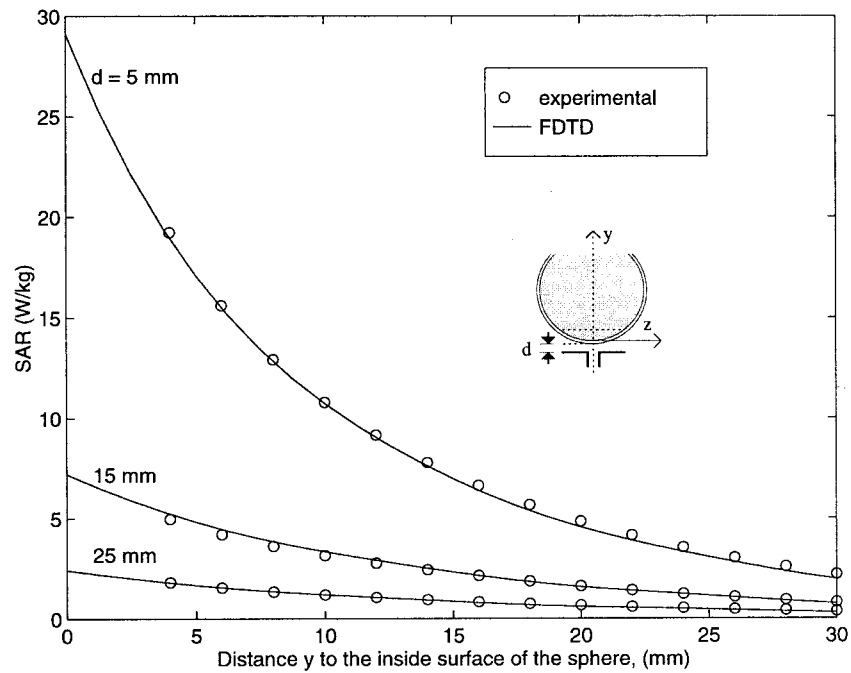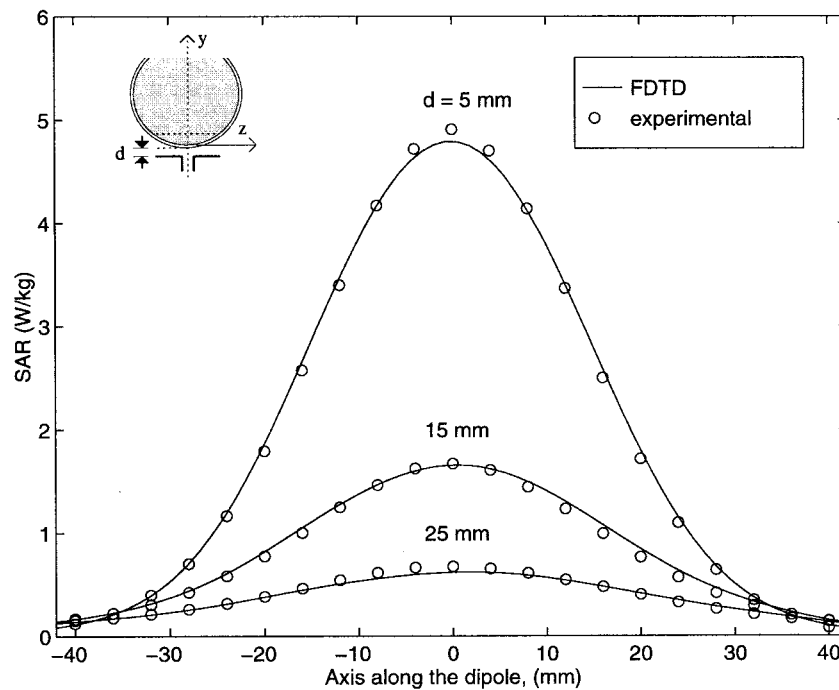
(a)
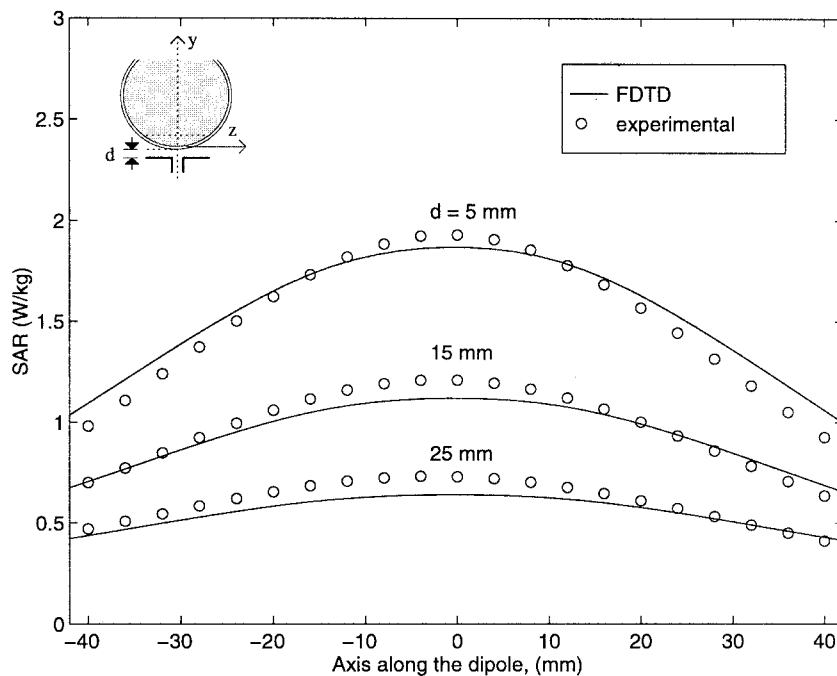
(b)

Fig. 6.   Comparison of measured and FDTD calculated SAR variations at 835 MHz for a glass sphere model of outer diameter 22.3 cm and thickness 5 mm. SAR's normalized to a radiated power of 0.5 W. (a) Variation of SAR along the y axis. (b) For a plane at a distance of 20 mm from the lowest point on the inside of the sphere.

there are excellent agreements between the calculated SAR's and the measured variations of the voltage output of the E-field probe for four different separations d of the half-wave dipoles at each of the two frequencies, it is possible to calculate the calibration factors at the respective frequencies by fitting the measured data to the FDTD calculated results by means of the least mean square error method. For the Narda Model 8021 E-field probe used in our setup, the calibration factors are determined to be 0.39 and 0.565 (mW/kg)/μV at 835 and 1900 MHz, respectively. It should be recognized that there would be some variability in the sensitivity of the diodes used for the various units of the Narda Model 8021 E-field probes. This calibration procedure using a box phantom may, therefore, be used to obtain the new calibration factors for each of the E-field probes.

(a)

(b)

Fig. 7.   Comparison of measured and FDTD calculated SAR variations at 1900 MHz for a glass sphere model of outer diameter 22.3 cm and thickness 5 mm. SAR's normalized to a radiated power of 0.5 W. (a) Variation of SAR along the y axis. (b) For a plane at a distance of 20 mm from the lowest point on the inside of the sphere. SAR's normalized to a radiated power of 0.5 W. Calibration factor $= 0.565$ (mW/kg)/μV. Measured for the phantom material $\varepsilon_r = 45.5$, $\sigma = 1.31$ S/m.

III. EXPERIMENTAL RESULTS: CANONICAL PROBLEMS

To further validate the SAR measurement system, it has been used to measure the peak 1-g SAR for the abovementioned box phantom and a glass sphere model of thickness 5 mm, external diameter $= 223$ mm and dielectric constant $\varepsilon_r = 4.0$. This sphere model is once again filled with the corresponding brain-simulant fluids of compositions given in Table II at 835 and 1900 MHz, respectively. Shown in Figs. 6(a) and (b) and 7(a) and (b) are the measured and FDTD calculated SAR distributions inside the sphere for various separations d between the dipole and the sphere (see insert for Figs. 6 and 7). Comparison of the measured and FDTD-

TABLE IV
Box Phantom:
Comparison of the Measured and FDTD Calculated Peal 1-g SAR's for
Four Spacings Each at 835 and 1900 MHz Radiated Power Normalized to 0.5 W

Frequency (MHz)	Distance (mm) between λ/2 dipole and the Box	SAR (W/kg)		Difference (%)
		Measured	FDTD	
835	17.5	4.58	4.20	+8.3
835	22.5	3.53	3.65	-3.4
835	27.5	2.69	3.00	-10.2
835	33.0	1.95	2.24	-12.9
1900	16.5	7.45	7.46	-0.1
1900	21.5	4.24	4.18	+1.4
1900	26.5	2.71	2.91	-7.9
1900	31.5	1.77	1.75	+1.1

TABLE V
Sphere Phantom:
Comparison of the Measured and FDTD-Calculated Peak 1-g SAR's for Three
Spacings Each at 835 and 1900 MHz, Radiated Power Normalized to 0.5 W

Frequency (MHz)	Distance (mm) between λ/2 dipole and the sphere	SAR (W/kg)		Difference (%)
		Measured	FDTD	
835	5	6.78	6.77	+0.23
835	15	3.41	3.27	+4.22
835	25	1.85	1.68	+9.51
1900	5	17.45	18.01	−3.21
1900	15	4.96	5.05	−1.81
1900	25	1.69	1.77	−4.73

calculated peak 1-g SAR's for both phantom geometries are given in Tables IV and V, respectively. As can be seen, the agreement between experimental measurement and numerical simulation is very good and generally within ±10% for both the rectangular and spherical phantoms.

IV. SAR Measurements for Cellular Telephones

The automated setup shown in Fig. 1 has been used for testing of ten personal wireless devices five each at 835 and 1900 MHz, respectively. Given in Table VI is the comparison of the numerical and measured peak 1-g SAR's for these devices using our experimental phantom model and the FDTD-based numerical procedure used for calculations of SAR distributions for an anatomically based model of the head of an adult male. The procedure for determining the peak 1-g SAR using the FDTD method with anatomical model has previously

been detailed in our earlier publications [2], [10]. Like the experimental method, it too relies on the determination of the averaged SAR for a volume of dimensions approximately $1 \times 1 \times 1$ cm with a mass as close to 1 g as possible. The measured and calculated SAR's for the ten telephones, which have quite different operational modes (time division multiple access [TDMA] or code division multiple access [CDMA]) and antenna structures (helical, monopole, or helix-monopole) vary from 0.13 to 5.41 W/kg. Even though widely different peak 1-g SAR's are obtained because of the variety of antennas and handsets, agreement between the calculated and the measured data is good and generally within ±20% (±1 dB). This is remarkable since a magnetic resonance image (MRI) derived, 15-tissue anatomically based model of the adult human head is used for FDTD calculations and a relatively simplistic two tissue phantom model is used for experimental peak 1-g SAR measurements. It is interesting to note that even

TABLE VI
COMPARISON OF THE EXPERIMENTALLY MEASURED AND FDTD-CALCULATED PEAK 1-g SAR'S
FOR TEN COMMERCIAL WIRELESS DEVICES, FIVE EACH AT 835 AND 1900 MHz, RESPECTIVELY

	Time-Averaged Radiated Power mW	Experimental Method W/kg	Numerical Method W/kg
Cellular Telephones at 835 MHz			
Telephone A	600	4.02	3.90
Telephone B	600	5.41	4.55
Telephone C	600	4.48	3.52
Telephone D	600	3.21	2.80
Telephone E	600	0.54	0.53
PCS Telephones at 1900 MHz			
Telephone A'	125	1.48	1.47
Telephone B'	125	0.13	0.15
Telephone C'	125	0.65	0.81
Telephone D'	125	1.32	1.56
Telephone E'	99.3	1.41	1.25

though the dielectric properties of the external shell (Fig. 1) are not as high as for the living human skull (see Table I), the peak 1-g SAR's obtained with this experimental phantom model agree quite well for the ten telephones used to date for which both the numerical and experimental procedures have been used.

V. CONCLUSIONS

An automated SAR measurement system has been developed with a dynamic range (0.01–10 W/kg) suitable for the compliance testing of personal wireless devices. This system uses a thick lossy shell of KCl-laced epoxy of 3–7 mm thickness to simulate the thickness of the human skull in the region of the maximum SAR's, i.e, the ear and the cheek. Unlike the previously reported thin-shell lossless ear phantoms [6], [7], the accuracy of this experimental phantom has been checked by comparing the peak 1-g SAR's for ten cellular telephones, five each at 835 and 1900 MHz, with the 1-g SAR's obtained using a 15-tissue anatomically based model with the FDTD numerical electromagnetic technique. Peak 1-g SAR's for these ten telephones using monopole, helix, or helix-monopole antennas are within ±1 dB of those obtained using the FDTD method for the anatomical model of the human body [2].

REFERENCES

[1] FCC 96-326, "Guidelines for evaluating the environmental effects of radio frequency radiation," FCC, Washington, DC 20554, Aug. 1, 1996.

[2] O. P. Gandhi, G. Lazzi, and C. M. Furse, "Electromagnetic absorption in the human head and neck for mobile telephones at 835 and 1900 MHz," *IEEE Trans. Microwave Theory Tech.,* vol. 44, pp. 1884–1897, Oct. 1996.

[3] G. Lazzi and O. P. Gandhi, "On modeling and personal dosimetry of cellular telephone helical antennas with the FDTD code," *IEEE Trans. Antennas Propagat.,* vol. 46, pp. 525–529, Apr. 1998.

[4] O. P. Gandhi and J. Y. Chen, "Electromagnetic absorption in the human head from experimental 6-GHz transceivers," *IEEE Trans. Electromagn. Compat.,* vol. 37, pp. 547–558, Nov. 1995.

[5] M. A. Jensen and Y. Rahmat-Samii, "EM interaction in handset antennas and a human in personal communications," *Proc. IEEE,* vol. 83, pp. 7–17, Jan. 1995.

[6] Q. Balzano, O. Garay, and T. J. Manning, Jr., "Electromagnetic energy exposure of simulated users of portable cellular telephones," *IEEE Trans. Veh. Technol.,* vol. 44, pp. 390–403, 1995.

[7] T. Schmid, O. Egger, and N. Kuster, "Automated E-field scanning system for dosimetric assessments," *IEEE Trans. Microwave Theory Tech.,* vol. 44, pp. 105–113, Jan. 1996.

[8] A. D. Tinniswood, C. M. Furse, and O. P. Gandhi, "Computations of SAR distributions for two anatomically-based models of the human head using CAD files of commercial telephones and the parallelized FDTD code," *IEEE Trans. Antennas Propagat.,* vol. 46, pp. 829–833, June 1998.

[9] B. Q. Gao and O. P. Gandhi, "An expanding-grid algorithm for the finite-difference time-domain method," *IEEE Trans. Electromagn. Compat.,* vol. 34, pp. 277–283, Aug. 1992.

[10] G. Lazzi and O. P. Gandhi, "Realistically tilted and truncated anatomically-based models of the human head for dosimetry of mobile telephones," *IEEE Trans. Electromagn. Compat.,* vol. 39, pp. 55–61, Feb. 1997.

[11] M. A. Stuchly and S. S. Stuchly, "Experimental radio and microwave dosimetry," in *Handbook of Biological Effects of Electromagnetic Fields,* 2nd ed., C. Polk and E. Postow, Eds. Boca Raton, FL: CRC, 1996, pp. 295–336.

[12] C. Gabriel, "Compilation of the dielectric properties of body tissues at RF and microwave frequencies," U.S. Air Force Armstrong Laboratory, Rep. AL/OE-TR-1996-0037, Brooks Air Force Base, TX 78235, June 1996.

[13] G. Hartsgrove, A. Kraszewski, and A. Surowiec, "Simulated biological materials for electromagnetic absorption studies," *Bioelectromagn.,* vol. 8, pp. 29–36, 1987.

[14] H. I. Bassen and G. S. Smith, "Electric field probes 3/4 a review," *IEEE Trans. Antennas Propagat.,* vol. AP-3, pp. 710–718, Sept. 1983.

[15] D. Hill, "Waveguide techniques for the calibration of miniature electric field probes for use in microwave bioeffects studies," *IEEE Trans. Microwave Theory Tech.,* vol. MTT-30, pp. 92–94, 1982.

[16] N. Kuster and Q. Balzano, "Energy absorption mechanism by biological bodies in the near field of dipole antennas above 300 MHz," *IEEE Trans. Veh. Technol.,* vol. 41, pp. 17–23, Feb. 1992.

[17] M. A. Stuchly, S. S. Stuchly, and A. Kraszewski, "Implantable electric field probes—Some performance characteristics," *IEEE Trans. Biomed. Eng.,* vol. BME-31, pp. 526–531, July 1984.

[18] A. Taflove, K. R. Umashankar, and T. G. Jurgens, "Validation of FDTD modeling of the radar cross section of three-dimensional structures spanning up to nine wavelengths," *IEEE Trans. Antennas Propagat.*, vol. AP-33, pp. 662–666, June 1985.

[19] C. M. Furse, Q. Yu, and O. P. Gandhi, "Validation of the finite-difference time-domain method for near-field bioelectromagnetic simulations," *Microwave Opt. Technol. Lett.*, vol. 16, pp. 341–345, Dec. 1997.

Magnus Aronsson (S'96) was born in Stockholm, Sweden, on March 25, 1973. He received the B.S. degree (*magna cum laude*) in electrical engineering from the University of Utah, Salt Lake City, in 1997. He is currently pursuing the M.S. degree in electrical engineering at the same university.

Since 1997, he has been a Research Assistant at the bioelectromagnetics group, University of Utah.

Qishan Yu was born in Shandong, China, in 1967. He received the B.S. and M.S. degrees in physics from Peking University, China, in 1985 and 1992, respectively.

Since 1996, he has been a graduate student in the Electrical Engineering Department, University of Utah, Salt Lake City, and has worked as a Research Assistant in the Bioelectromagnetics Laboratory, Electrical Engineering Department, at the same university.

Ding Wu, photograph and biography not available at the time of publication.

Om P. Gandhi (M'58–SM'65–F'79–LF'99) is a Professor and the Chairman of the Department of Electrical Engineering, University of Utah, Salt Lake City. He is the author or coauthor of several book chapters and journal articles on electromagnetic dosimetry, microwave tubes, and solid-state devices. He also recently edited *Biological Effects and Medical Applications of Electromagnetic Energy* (Englewood Cliffs, NJ: Prentice-Hall, 1990) and coedited *Electromagnetic Biointeraction* (New York: Plenum, 1989).

Dr. Gandhi received the Distinguished Research Award from the University of Utah (1979–1980) and a special award for Outstanding Technical Achievement from the IEEE, Utah Section, in 1975. He has been co-chairman of IEEE SCC 28.IV subcommittee on RF safety standards (1988–1997), served as Vice President/President of the Bioelectromagnetics Society (1991–1993), and as chairman of the IEEE Committee on Man and Radiation (COMAR) (1980–1982). In 1995 he received the d'Arsonval Medal of the Bioelectromagnetics Society for pioneering contributions to the field of bioelectromagnetics. He is listed in *Who's Who in the World*, *Who's Who in America*, *Who's Who in Engineering*, and *Who's Who in Technology Today*.